AAV delivery of RNA editing machinery rescues SUDEP and seizure phenotype in a mouse model of Dravet Syndrome

Ellie M. Chilcott[1], Juan F. Antinao Diaz[1], Amanda Almacellas Barbanoj[2], Marc Moore[3], Anna Keegan[1], Zakary Waddington[1], Vicky Fang[1], Stephanie Schorge[4], Gabriele Lignani[2], Simon N Waddington[1] & Rajvinder Karda[1*]

Affiliations

[1] EGA Institute for Women's Health, University College London, 86-96 Chenies Mews, London, WC1E 6HX, UK

[2] Queen Square Institute of Neurology, Queens Square, University College London, London, WC1N 3BG, UK

[3] School of Health and Life Sciences, National Horizon Centre, Teesside University, 38 John Dixon Ln, Darlington, DL1 1HG, UK

[4] Division of Biosciences, Medical Science Building, University College London, London WC1E 6BT

[*]Corresponding author: Dr Rajvinder Karda
Maternal and Fetal Medicine Department
Institute For Women's Health
University College London
86-96 Chenies Mews
WC1E 6HX
London
r.karda@ucl.ac.uk

Key words: Adeno-associate virus, RNA editing, CIRTS (CRISPR-Cas-inspired RNA targeting system), preclinical, Dravet Syndrome

ABSTRACT

Dravet syndrome (DS) is a severe childhood genetic epilepsy, caused by *de novo* heterozygous mutations in *SCN1A*, resulting in a loss-of-function of the voltage-gated sodium ion channel, Nav1.1. Nav1.1 is expressed in the brain, and at a lower level, in the heart. DS manifests in the first year of life. Patients exhibit tonic-clonic seizures, febrile seizures, cognitive decline, developmental delays, ataxia, and sudden unexpected death from epilepsy (SUDEP). We have developed a novel AAV-F mediated CRISPR-Cas-inspired RNA targeting system (CIRTS) preclinical treatment to increase endogenous *Scn1a* and ameliorate the disease phenotype in a clinically-relevant heterozygous loss-of-function mouse model of DS. We designed novel guide RNAs (gRNAs) to target the long non-coding RNA, (or natural antisense transcript) of *Scn1a* to increase the expression of *Scn1a* mRNA in DS mice. We show that intracerebroventricular and intravenous administration of AAV-F-CIRTS-gRNA9 to target the brain and the heart to neonatal $Scn1a^{+/-}$ mice resulted in a significant increase in survival, and a reduction in SUDEP, febrile seizures and seizure duration. These findings provide proof-of-concept evidence that an AAV-F-CIRTS mediated therapy hold promise as a potential treatment for DS.

INTRODUCTION

Dravet syndrome (DS) is a severe childhood genetic epilepsy, with an incidence rate of 1 in 15,400-40,900 live births worldwide*(1, 2)*. The disease typically manifests within the first year of life accompanied by tonic-clonic seizures, febrile and afebrile seizures, episodes of status epilepticus, cognitive impairment, ataxia and unfortunately, ~15% of patients experience sudden unexpected death in epilepsy (SUDEP)*(3–5)*. >90% of patients harbour *de novo* loss-of-function variants in the *SCN1A* gene which encodes an α-subunit of a voltage-gated ion channel, Nav1.1*(6)*. In humans, Nav1.1 expression has been detected in the hippocampus (including the

60 dentate gyrus, CA3, and CA2 regions), layers V and VI of the cortex, the granular and molecular
61 layers, as well as in the deep nuclei and Purkinje cells of the cerebellum*(7)* and the
62 heart. Previous studies have explored altered cardiac function in individuals with DS and in
63 mouse models, suggesting a potential contribution to SUDEP*(8–11)*.

64 Current anti-seizure medications, including valproate, stiripentol, fenfluramine and
65 cannabidiol can reduce the seizure frequency*(12)*, but the disease manifestation continues. Thus,
66 there remains a significant unmet need to establish an effective long-term treatment for DS.

67 Adeno-associated viral (AAV) vectors, specifically AAV9, have been used extensively
68 for many preclinical*(13, 14)* and clinical trials*(15, 16)*. However, the high doses of AAV9
69 required to achieve efficacious peripheral delivery has also caused liver toxicity and thrombotic
70 microangiopathy*(16, 17)*. As such, there is a need to develop novel capsids that enable efficient
71 therapeutic delivery at a lower dose, avoiding immunotoxicity associated with the gene therapy
72 vector. Novel AAV capsids targeting the central nervous system (CNS) have been generated*(18,*
73 *19)*. One example of this is AAV-F, a novel capsid derived from AAV9, which has shown a
74 greater CNS transduction efficiency relative to the parental AAV9 capsid*(18)*.

75 RNA targeting technologies have emerged as therapeutic, inspired by successes in
76 oligonucleotide based therapies*(20, 21)*. Targeting RNA is advantageous over DNA as it can
77 influence gene expression without permanent alterations to the host genome and modulate
78 protein expression regardless of the specific mutation. Furthermore, DNA and RNA targeting
79 systems such as Cas9 and Cas13 are built from bacterial proteins and have shown to induce an
80 immune response *in vivo(22)*. A new RNA editing technology has been developed to target RNA
81 sequences, referred to as CRISPR-Cas-inspired RNA targeting system (CIRTS)*(23)*. CIRTS is
82 built from human proteins and previous validation studies *in vitro* and *in vivo* have shown the

83 CIRTS system to modulate protein expression by RNA editing *(23–25)*, although until now this
84 has not been used in a therapeutic setting. In this study, we used a CIRTS construct consisting of
85 a ssRNA binding protein (β-defensin 3), RNA hairpin-binding protein (TBP6.7) and effector
86 protein (YTHDF2)*(23)* to down-regulate target RNA expression.

87 Here, we used the AAV-F-mediated CIRTS technology and designed novel guide RNAs
88 (gRNAs) to edit a *Scn1a* specific long non-coding RNA (lncRNA) of the natural antisense
89 transcript (NAT), which normally functions to negatively regulate *Scn1a* expression*(26)*. In
90 doing so, we aimed to 'inhibit the inhibitor', leading to an upregulation of *Scn1a* mRNA (Fig.
91 1A). We screened 21 gRNAs *in vitro* and selected two lead candidate gRNAs (gRNA9 & 21)
92 which significantly increased endogenous *Scn1a* mRNA and shared highest homology to the
93 human lncRNA sequence. We used a clinically-relevant DS heterozygous (*Scn1a*$^{+/-}$) model,
94 which recapitulates much of the human disease, including spontaneous and febrile seizures, and
95 SUDEP*(27, 28)*. We administered our candidates AAV-F-CIRTS-gRNA 9 & 21 vectors to
96 neonatal DS mice via intracerebroventricular (ICV) and intravenous (IV) administration to target
97 the brain and the heart. Candidate AAV-F-CIRTS-gRNA9 resulted in significant increase in
98 survival over 100 days post-injection. In addition, febrile and spontaneous seizure assessment of
99 DS mice injected with AAV-F-CIRTS-gRNA9 showed a significant reduction in seizure severity
100 and seizure duration. Molecular analysis revealed a significant up-regulation of endogenous
101 *Scn1a* mRNA in treated AAV-F-CIRTS-gRNA9 DS mice compared to untreated DS control
102 mice. Our work demonstrates for the first time, a potential AAV-F mediated RNA editing
103 approach to treat patients with DS.

104

105

106 **RESULTS**

107 **Design and *in vitro* validation of novel gRNAs targeting *Scn1a* lncRNA**

108 We firstly validated the CIRTS machinery and consistent with previous studies*(23)*,
109 AAV-CIRTS-gRNAluc was able to significantly reduce luciferase expression (Fig. S1A). We
110 designed 21 novel gRNA sequences (20-30mer) to target the *Scn1a* lncRNA (Fig. 1A) (here
111 referred to as *Scn1anat*), which were cloned into the AAV-CIRTS plasmid (Fig. 1B). We
112 validated our gRNA designs *in vitro*, in differentiated mouse Neuro2a cells and assessed the
113 effects on endogenous *Scn1a* mRNA expression. Transient transfection of AAV-CIRTS-gRNA
114 constructs onto differentiated Neuro2a cells resulted in a significant increase of endogenous
115 *Scn1a* mRNA by 4 out of 21 AAV-CIRTS-gRNA constructs (Fig. 1C). Constructs containing
116 gRNAs 9, 11, 15 and 21 led to average *Scn1a* mRNA fold changes of 1.89 (P=0.0016), 2.15
117 (P=0.0015), 2.12 (P=0.022) and 2.56 (P<0.0001), respectively. gRNAs 9 and 21 were selected
118 for the *in vivo* study as they showed the highest homology to the *SCN1A* lncRNA (*SCN1ANAT*;
119 93.3% and 100%, respectively) (Fig. 1C).

120

121 **AAV-F-mediated RNA editing in DS mice significantly improves survival**

122 In this study we crossed the males from 129Sv-*Scn1a*^{tm1Kea}/Mmjax model*(27, 28)* with
123 wild-type CD1 females to generate F2 129Sv-*Scn1a*^{tm1Kea}/Mmjax x CD1 heterozygote females,
124 which were then bred to wild-type C57BL/6J males to obtain experimental litters (*Scn1a*$^{+/-}$). This
125 enabled a larger litter size. *Scn1a*$^{+/-}$ mice exhibit spontaneous seizures and SUDEP with an
126 overall survival of 38.2% over 100 days of development (Fig. S2A), febrile seizures (Fig. S2D)
127 and a reduction in *Scn1a* gene expression, particularly in the cortex at P50 (P=0.0078; Fig. S2E),

128 consistent with previous studies*(21, 27, 29)*. RNA-seq of *Scn1a*$^{+/+}$ and *Scn1a*$^{+/-}$ cortical tissue at
129 P50 confirmed 140 up- and 41 down-regulated genes (Fig. S3A and B), with significant down-
130 regulation of *Scn1a* (-0.77Log2FC, P=5.85x10^{-6}; Fig. S2C). Molecular function gene ontology
131 (GO) analysis of the differentially expressed genes in *Scn1a*$^{+/-}$ mice reveal up-regulation in terms
132 related to neuropeptide receptor activity, monoatomic ion transport and voltage-gated sodium
133 channel activity (Fig. S3D).

134 Using this DS mouse model, we sought to determine the optimal capsid and gRNA
135 combination by generating AAV-F and AAV9 vectors for AAV-CIRTS-gRNA9 and AAV-
136 CIRTS-gRNA21, using AAV9 as a gold-standard comparison. At P0, *Scn1a*$^{+/-}$ mice received an
137 intracerebroventricular (ICV) and intravenous (IV) delivery of either AAV-F (7x10^{10} vg/pup) or
138 AAV9 (7x10^{11} vg/pup), each encoding either gRNA9 or 21 to determine the effects on survival.
139 This study was fully blinded and randomised (Fig. 2A). AAV-F vectors were injected at 10-fold
140 lower dose than AAV9. PBS-injected *Scn1a*$^{+/+}$ and *Scn1a*$^{+/-}$ mice served as controls. *Scn1a*$^{+/-}$
141 mice treated with AAV-F-CIRTS-gRNA9 had a significant (P=0.0235) increase in overall
142 survival to 70.4% at P100 compared to 36.4% survival at P100 in PBS-treated *Scn1a*$^{+/-}$ controls
143 (Fig. 3A and Fig. S3B). In contrast, AAV9-CIRTS-gRNA9 only showed an overall survival of
144 26.5% (P=0.8439, Fig. S2B). The AAV-F-CIRTS-gRNA21 treatment group also appeared less
145 efficient, showing only a 12.5% survival (P=0.0509, Fig. S4A), while AAV9-CIRTS-gRNA21
146 had a 50% survival at P100 (P=0.3715, Fig. S4A). Weights and open field analysis of neither
147 AAV-F- or AAV9-CIRTS-gRNA9/21 treated mice differed from PBS *Scn1a*$^{+/+}$ and *Scn1a*$^{+/-}$
148 control group (Fig. 2C and D & Fig. S4B, C and D). From these data, AAV9 RNA editing at a
149 10-fold higher titre than AAV-F failed to improve survival we therefore, proceeded with AAV-
150 F-CIRTS-gRNA9 for the remaining experiment.

151 We interrogated dose-range efficacy of AAV-F-CIRTS-gRNA9 with one higher and one
152 lower dose. High dose ($1.75x10^{11}$ vg/pup) resulted in 65.5% survival (P=0.0732, Fig. 3A), whilst
153 low dose ($1.75x10^{10}$ vg/pup) resulted in 44.4% survival, compared to PBS-treated *Scn1a*$^{+/-}$ mice
154 over 100 days (P=0.5815 and P=0.8556, respectively, Fig. 3A). Neither of the additional AAV-
155 F-CIRTS-gRNA9 doses were superior to our originally tested dose of $7x10^{10}$ vg/pup.
156 Furthermore, no doses showed difference in weight or open field assessment compared to PBS
157 *Scn1a*$^{+/+}$ control group (Fig. 3B, C and Fig. S5A).

158

159 **AAV-F-CIRTS-gRNA9 reduces seizure burden in DS mice**

160 To assess the effects of this optimal dose of AAV-F-CIRTS-gRNA9 therapy on febrile
161 and spontaneous seizures in *Scn1a*$^{+/-}$ mice, we administered a separate cohort of *Scn1a*$^{+/-}$ mice
162 with neonatal ICV and IV delivery ($7x10^{10}$ vg/pup). We also administered control groups AAV-
163 F-CIRTS-gRNAluc ($7x10^{10}$ vg/pup) and PBS to neonatal *Scn1a*$^{+/-}$ mice via ICV and IV delivery
164 (Fig. 4A). Febrile seizure assessment revealed a significant improvement in seizure severity
165 determined by the Racine scale*(30)* (Fig. 4B), in AAV-F-CIRTS-gRNA9 treated *Scn1a*$^{+/-}$ mice
166 compared to PBS *Scn1a*$^{+/-}$ control group (P<0.0001; Fig. 4B), and AAV-F-CIRTS-gRNAluc
167 *Scn1a*$^{+/-}$ control group (P=0.0111; Fig. 4B).

168 Electroencephalogram (EEG) recordings of spontaneous seizures were recorded for 15
169 days between P30-45 and the results revealed a trend to reduction of seizure burden in AAV-F-
170 CIRTS-gRNA9 mice, compared to a control AAV-F-CIRTS-gRNAluc. Total numbers of
171 seizures (9.7±13 vs 4.1±7.3; P=0.4121; Fig. S7A) and average numbers of seizures per day
172 (0.78±0.93 vs 0.33±0.48; P=0.43; Fig. S7B) were reduced. In the mice which displayed seizures,
173 the average seizure duration was significantly reduced in the treated AAV-F-CIRTS-gRNA9

174 *Scn1a*$^{+/-}$ group compared to control AAV-F-CIRTS-gRNAluc *Scn1a*$^{+/-}$ group (P=0.0279; Fig.
175 4D), as well as a trend for reduction in cumulative seizure time (P=0.0640; Fig. S7C).

176

177 **AAV-F-CIRTS-gRNA9 normalises molecular signature of DS**

178 To determine the effects of AAV-F-CIRTS-gRNA9 on endogenous *Scn1a* mRNA, we
179 assessed gene expression in the cortex and the heart of treated *Scn1a*$^{+/-}$ mice. Raw wild-type
180 *Scn1a* gene expression levels were restored in both the cortex and heart of AAV-F-CIRTS-
181 gRNA9 mice (P=0.0072 and P=0.0002 vs PBS *Scn1a*$^{+/-}$; Fig. 5A and B).

182 Vector copy number (VCN) assessing the presence of the effector protein *YTHDF2*
183 genomic sequence, showed an increase in both *Scn1a*$^{+/-}$ and *Scn1a*$^{+/+}$ mice treated with AAV-F-
184 CIRTS-gRNA9 treated mice in the cortex at P100 compared to both PBS (P=0.0014) and AAV-
185 F-CIRTS-gRNAluc (P=0.0146) groups *Scn1a*$^{+/+}$ (VCN 0.35±0.44; Fig. 5C). No difference was
186 observed in the heart and the liver (VCN 0.19±0.14 and 0.04±0.05, respectively; Fig. 5C).
187 *YTHDF2* mRNA expression mimicked the pattern of vector copy number with highest
188 expression in the cortex in AAV-F-CIRTS-gRNA9 *Scn1a*$^{+/-}$ mice. No significance was observed
189 in the heart and the liver (Fig. S8A).

190

191 ***In vivo* safety of AAV-F-CIRTS-gRNA9**

192 Both AAV-F-CIRTS-gRNA9 and AAV-F-CIRTS-gRNAluc were injected to *Scn1a*$^{+/+}$
193 mice at the two highest dosages 1.75×10^{11} vg/pup and 7×10^{10} vg/pup via neonatal ICV and IV to
194 determine any toxicological findings. No adverse effects on survival or weight were seen (Fig.
195 S9A and B). Open field analyses revealed hyperactivity in the total distance of *Scn1a*$^{+/+}$ AAV-F-

196 CIRTS-gRNAluc mice treated with dose $1.75x10^{11}$ vg/pup at P18 and P55 (P=0.0003, P=0.0217;
197 Fig. S9C), also with an increase in maximum speed at P55 (P=0.0099; Fig. S9D) compared to
198 PBS *Scn1a*$^{+/+}$ control group.

199 Immunohistochemical analysis to detect astrocytes (GFAP) and macrophages, including
200 kupffer cells, in the brain and liver respectively was performed post-AAV-F-CIRTS-gRNA9
201 treatment. No increases in reactive astrocytes were seen in the brains of treated *Scn1a*$^{+/+}$ or
202 *Scn1a*$^{+/-}$ mice (Fig. 6A and B). An increase in the presence of macrophages/kupffer cells in the
203 liver was seen in only the *Scn1a*$^{+/+}$ mice treated with AAV-F-CIRTS-gRNAluc (P=0.0025), this
204 was not observed in mice of either genotype treated with the same dose of AAV-F-CIRTS-
205 gRNA9 (Fig. 6A and C).

206

207 ***In vivo* editing specificity of AAV-F-CIRTS-gRNA9**

208 To identify gRNA-specific changes in gene expression, we conducted RNA-seq on
209 cortical tissue 50 days post-injection and compared AAV-F-CIRTS-gRNAluc and AAV-F-
210 CIRTS-gRNA9 *Scn1a*$^{+/-}$ mice. Only 9 differentially expressed genes were found; 3 up-regulated
211 and 6 down-regulated (Fig. 7A and B). Of note, inflammation-associated genes were down-
212 regulated including *Igkc* (-7.27Log2FC, P=0.0417), *Cxcl13* (-7.35Log2FC, P=0.0417) and *Adgre*
213 (-1.86Log2FC, P=0.0019) and the only driver GO term changed across the comparison, was the
214 down-regulation of CXCR5 chemokine receptor binding (Fig. 7C; P=0.0499). None of the *Scna*
215 genes, which encode other voltage-gated sodium ion channels, were differentially expressed in
216 the gRNA9 group compared to gRNAluc.

217

218

219 **DISCUSSION**

220 Here, we provide preclinical proof-of-concept data demonstrating that CIRTS-mediated
221 RNA editing can mitigate the phenotype of a severe neurological disorder, Dravet syndrome. A
222 single administration of AAV-F-CIRTS-gRNA9 by combined ICV and IV delivery to *Scn1a*$^{+/-}$
223 DS mice induces destruction of *Scn1anat* and completely rescues endogenous *Scn1a* mRNA
224 expression in both the cortex and the heart. This was shown to improve disease manifestation by
225 reducing febrile seizure severity and significantly reducing SUDEP, with minimal off-target
226 effects; whilst being compromised entirely of human components.

227 We designed the gRNAs used in this study with the aim of restoring wild-type *Scn1a*
228 expression levels, without leading to supraphysiological expression. Notably, modest 2.6- and
229 1.9-fold increase of *Scn1a* expression *in vitro* were achieved with gRNA21 and gRNA9
230 respectively. We sought to combine these with AAV-F, an engineered capsid, shown to have a
231 more efficient CNS transduction profile than AAV9 in rodents*(31)*, human neurons*(31)* and
232 NHPs*(19)*. By packaging AAV-CIRTS-gRNA9 into AAV-F and AAV9 we demonstrated vastly
233 different therapeutic effects with 70.4% and 26.5% survival, respectively, strikingly this was
234 achieved with AAV-F being administered at a 10-fold lower dose. However, gRNA21 delivered
235 by either AAV-F or AAV9 did not reveal a significant improvement in survival. We tested a
236 varying dose of AAV-F-CIRTS-gRNA9 and determined that $7x10^{10}$ vg/pup achieved a
237 significant survival of 70.4% at P100, interestingly increasing the dose further to $1.75x10^{11}$
238 vg/pups showed a reduced survival of 65.5% over 100 days. These findings suggest a narrow
239 therapeutic dose ranging window for a successful treatment for DS. This is particularly important
240 in the context of *SCN1A*, as gain-of-function *SCN1A* variants, which are known to cause familial
241 hemiplegic migraine type 3 and a severe infantile developmental and encephalopathy (distinct

242 from DS) with associated movement disorder*(32)*. Therefore, future studies require a more
243 refined dose ranging evaluation of AAV-F with gRNA9 or gRNA21 to determine the optimal
244 therapeutic dose, with appropriate levels of physiological *Scn1a* and no behavioural side effects.

245 As a main symptom of DS is seizures, we sought to assess the seizure activity in our
246 AAV-F-CIRTS-gRNA9 treated *Scn1a*$^{+/-}$ DS mice via febrile seizure assessment and EEG
247 monitoring for 15 days (P30-45). We delivered a vehicle and control vector AAV-F-CIRTS-
248 gRNAluc to *Scn1a*$^{+/-}$ DS mice as a comparators. Febrile seizure assessment revealed a
249 significant reduction in seizure severity determined by the Racine scale in AAV-F-CIRTS-
250 gRNA9 treated *Scn1a*$^{+/-}$ mice compared to PBS and AAV-F-CIRTS-gRNAluc *Scn1a*$^{+/-}$ control
251 group. EEG seizure monitoring was performed for AAV-F-CIRTS-gRNA9 and AAV-F-CIRTS-
252 gRNAluc treated *Scn1a*$^{+/-}$ DS mice. Our results showed that we could significantly reduce the
253 seizure duration in our treated *Scn1a*$^{+/-}$ DS mice. From these data, we observed a variability in
254 the AAV-F-CIRTS-gRNAluc *Scn1a*$^{+/-}$ DS mice, as some of these mice did not display seizures
255 during the EEG recording. Which may partly be due to the variable penetrance of spontaneous
256 seizures in this model*(33)*. This was a limitation in our study and future studies, will require
257 further power calculations to establish the appropriate number of *Scn1a*$^{+/-}$ mice required for EEG
258 seizure monitoring.

259 Molecular assessment revealed a significant increase in endogenous *Scn1a* mRNA in the
260 cortex and the heart of treated AAV-F-CIRTS-gRNA9 *Scn1a*$^{+/-}$ mice. Immunohistochemical
261 analysis in the brain of AAV-F-CIRTS-gRNA9 *Scn1a*$^{+/-}$ and *Scn1a*$^{+/+}$ mice showed no signs of
262 toxicity. Liver toxicity was only observed in AAV-F-CIRTS-gRNAluc *Scn1a*$^{+/+}$ treated group,
263 suggesting potential guide-specific side-effects of AAV-F-CIRTS-gRNAluc vector.

264 To determine the off-target effects of our gRNA9, we conducted RNA-seq on cortical
265 brain tissues for AAV-F-CIRTS-gRNAluc and AAV-F-CIRTS-gRNA9 *Scn1a*$^{+/-}$ treated mice.
266 The data revealed inflammation-associated genes including *Igkc(34)*, *Cxcl13(35)* and *Adgre(36)*
267 were down-regulated in the AAV-F-CIRTS-gRNA9 treated group. Previously, up-regulation of
268 the CXCL13-CXCR5 signalling pathway has been associated with intractable epilepsy*(35)*,
269 suggesting that our therapy may be able to reduce some molecular signatures of epilepsy
270 pathogenesis. Furthermore, our data suggest no off-target effects of the gRNA9 coupled with the
271 CIRTS machinery.

272 Several approaches in preclinical development have used genetic therapies specifically in
273 inhibitory interneurons using *SCN1A* gene replacement with split-intein dual AAVs*(37)* and
274 Adenoviral vectors*(38)*, CRISPR/dCas9 activation of *SCN1A(39, 40)* and transcription factor-
275 mediated *SCN1A* up-regulation*(29)*. While these approaches target the primary pathology of
276 Dravet syndrome (DS), our strategy complements these alternative therapeutic interventions by
277 also considering effects in less well-studied cell populations, such as cardiomyocytes*(10)*. Here,
278 we have shown that our AAV-F-CIRTS-gRNA9 can increase *Scn1a* mRNA in the cortex and the
279 heart.

280 *SCN1ANAT* has been detected in surgical brain tissue specimens from patients (1-19
281 years of age) undergoing resection to treat refractory, non-DS epilepsy*(41)*. Previous evidence
282 has shown that targeting *Scn1anat* using small oligonucleotides termed AntagoNATs were able
283 to reduce seizures and normalise neuronal activity in DS knock-in mice*(26)*. Furthermore, we
284 have also shown that these AntagoNATs can be vectorised with AAV9, which also demonstrates
285 a significant improvement in DS phenotype*(42)*. Here, we also are targeting *Scn1anat*, but
286 instead of blocking the interaction between this and the *Scn1a* mRNA, we are inducing the

287 degradation of *Scn1anat*, with similar phenotypic improvement. These findings demonstrate the
288 feasibility of using AAV mediated RNA editing to modulate *Scn1a* expression, highlighting its
289 potential as a therapeutic for DS.

290 Genetic therapies for DS have progressed to clinical evaluation. These include the
291 antisense oligonucleotide (ASO) zorevunersen, currently under investigation in Phase 1/2a
292 MONARCH and ADMIRAL trials, which involve repeated intrathecal administration*(43)*.
293 Encoded Therapeutics has developed an AAV9-based transcription factor*(29)* approach
294 specifically targeting GABAergic interneurons, now being assessed in a Phase 1/2 clinical trial
295 utilizing ICV delivery alone*(44)*. Similar to Encoded Therapeutics' strategy, our AAV-F-CIRTS-
296 gRNA9 platform offers a one-time treatment; however, it confers the additional advantage of
297 enabling broader targeting of CNS cell populations expressing Nav1.1. Furthermore, the
298 inclusion of IV administration is intended to achieve efficient cardiac transduction, addressing
299 evidence implicating altered cardiac electrophysiology*(8, 11)* in contributing to SUDEP.

300 Our study presented limitations. Some of the *Scn1a*$^{+/-}$ DS mice did not present seizures
301 during EEG recording and therefore, for future studies we will require further power
302 calculations. The future studies required have been detailed in this discussion.

303 In conclusion, we have developed and characterized an AAV-F-CIRTS RNA editing
304 therapeutic strategy for the treatment of DS. Incorporation of gRNA targeting *Scn1anat*
305 successfully modulated *Scn1a* expression and significantly improved survival, seizure severity
306 and duration in *Scn1a*$^{+/-}$ mice. These findings provide compelling proof-of-concept evidence
307 supporting the potential of this approach as a therapeutic intervention for DS.

308

309

310 **MATERIALS AND METHODS**

311 **Study design**

312 This study was designed to investigate if AAV-CIRTS-mediated RNA editing to induce
313 the destruction of *Scn1anat* could lead to therapeutic benefit in a clinically relevant DS mouse
314 model. The following design elements were included in this study. N=3 independent experiments
315 were conducted for *in vitro* gRNA screening experiments with at least n=3 technical replicates
316 per condition. Mice were assigned randomly to study groups, with at least one control (either
317 PBS or AAV-F-CIRTS-gRNAluc-treated) *Scn1a*$^{+/-}$ mouse per litter and remaining *Scn1a*$^{+/+}$ and
318 *Scn1a*$^{+/-}$ littermates mice treated with AAV-F-CIRTS-gRNA9/21 or AAV9-CIRTS-gRNA9/21
319 treated mouse. Prospectively selected endpoints of these studies were survival, weight, open
320 field, longitudinal gene expression and neuropathological analyses. Sample sizes for *in vivo*
321 experiments were not pre-defined before the outset of data collection as no preliminary data were
322 available to estimate effect sizes and thus be able to complete power analyses. *In vivo* studies
323 analysing seizures used *Scn1a*$^{+/-}$ littermates treated with AAV-F-CIRTS-gRNAluc as a non-
324 targeting guide as a control for AAV-F-CIRTS-gRNA9. At termination of the in-life period for
325 all *in vivo* experiments, mice were assigned a numeric code and investigators were blinded to
326 treatment and genotype whilst analysing tissue.

327 **gRNA design and cloning**

328 The *Scn1anat* target sequence was inputted into sOligo software
329 (https://sfold.wadsworth.org/cgi-bin/soligo.pl), varying the parameter for gRNA length. Folding
330 temperature was set to 37°C and ionic conditions set to 1M NaCl with no divalent ions.
331 Resulting outputs were screened for those with less than -8.0 Gibbs free energy with positional
332 clusters identified. Potential gRNA sequences were manually mapped to RNA secondary

333 structures produced using mFold software (http://www.unafold.org/mfold/applications/rna-
334 folding-form.php) to determine qualities of each gRNA such as the number of termini and
335 percentage of gRNA sequence in open conformation. gRNAs were cloned into the AAV-CIRTS
336 plasmid (Addgene plasmid #132544), using gBlocks from Integrated DNA Technologies and
337 InFusion cloning (Takara Bio). The AAV-CIRTS plasmid contains a cytomegalovirus promoter
338 (CMV), driving ssRNA binding protein β-defensin 3, RNA hairpin-binding protein (TBP6.7),
339 effector protein (YTHDF2) and U6 promoter driving gRNA (referred to as AAV-CIRTS in the
340 main text, Fig. 1B).

341 ***In vitro* analyses**

342 For luciferase assays; HEK293T cells ($5x10^4$ per well of 24-well plate) were transfected
343 with 0.8µg of an AAV plasmid containing an Spleen focus forming virus ubiquitous promoter
344 (SFFV) driving luciferase linked to green fluorescent reporter gene with a T2A linker
345 peptide*(45)* (referred to as AAV-SFFV-*luciferase*-T2A-*eGFP* in the main text) ± 0.8µg AAV-
346 CIRTS-gRNAluc using Lipofectamine 2000 (Thermo Fisher Scientific). Cells were lysed in
347 Luciferase Cell Culture Lysis Reagent (Promega) at 72h post-transfection, with half the lysate
348 used to determine protein concentration using the DC protein assay (BioRad). The remaining
349 half of the lysate was used for luminometry measured in a FLUOstar® Omega microplate
350 reader (BMG Labtech). Luciferase expression was normalised to protein concentration within
351 each sample.

352 For *Scn1anat* gRNA screening; Neuro2a cells ($3x10^4$ per well of 24-well plate) were
353 differentiated in DMEM (Thermo Fisher Scientific), 2% FCS (Sigma-Aldrich), 0.5mM cAMP
354 (Merck) and 20µM Retinoic Acid (Merck). At 6DIV, cells were transfected with 0.8µg AAV-
355 SFFV-*luciferase*-T2A-*eGFP* or AAV-CIRTS-gRNA1-21 using Lipofectamine 2000 (Thermo

356 Fisher Scientific). Cells were lysed in TRIzol reagent (Thermo Fisher Scientific) at 5d post-
357 transfection. RNA was extracted and qPCR used to determine changes in *Scn1a* gene expression
358 (protocols described below).

359 **AAV vector production**

360 Recombinant AAV vectors were produced by triple-transfection*(46)* of AAVpro 293T
361 cells (Takara Bio) with AAV-CIRTS, adenovirus helper plasmid (Harvard University) and either
362 AAV9 (University of Pennsylvania; Addgene #112865) or AAV-F (Harvard University,
363 Addgene #166921) capsid plasmids using PEImax (Polysciences Inc.). HPLC using POROS
364 CaptureSelect AAVX Resin (Thermo Fisher Scientific) was used to purify resulting vector
365 before being titrated by qPCR.

366 **Animals**

367 All procedures were performed in accordance with UK Home Office Animals (Scientific
368 Procedures) Act 1986 under PPLs 70/14300, PP8023218 & PP9223137. All mice were housed in
369 IVCs with enrichment, under a 12 hour:12 hour light–dark cycle and had access to food and
370 water *ad libitum*. The mouse model of Dravet syndrome used in this project is derived from the
371 129Sv-*Scn1a*^{tm1Kea}/Mmjax model*(27, 28)* (Jackson Laboratory) that has been extensively used in
372 DS pre-clinical research. Males from this strain were bred with wild-type CD1 females to obtain
373 a F1 129Sv-*Scn1a*^{tm1Kea}/Mmjax x CD1 generation. F1xF1 crosses were bred to obtain F2 129Sv-
374 *Scn1a*^{tm1Kea}/Mmjax x CD1 heterozygote females which were bred to wild-type C57BL/6J males
375 to obtain experimental litters (here referred to as *Scn1a*$^{+/-}$ in the text). Humane endpoints of
376 >15% weight loss, observation of two seizures and/or clear signs of illness (piloerection,
377 hunched posture and laboured breathing).

378 At post-natal day 0 (P0), *Scn1a*$^{+/-}$ pups were injected by bilateral intracerebroventricular
379 (ICV; 5 μL per hemisphere, using previously published coordinates*(47)*) and intravenous (IV; 25
380 μL via superficial temporal vein*(48)*) routes of administration with either PBS, AAV9 (total dose
381 $7x10^{11}$ vg/pup ($2x10^{11}$ vg ICV + $5x10^{11}$ vg IV)) or AAV-F (total dose $1.75x10^{10}$ vg/pup ($5x10^{9}$
382 vg ICV + $1.25x10^{10}$ vg IV), $7x10^{10}$ vg/pup ($2x10^{10}$ vg ICV + $5x10^{10}$ vg IV) and $1.75x10^{11}$
383 vg/pup ($5x10^{10}$ vg ICV + $1.25x10^{11}$ vg IV)) using a 33-gauge Hamilton needle (VWR). After the
384 procedure, mice were returned to their dams. Weight and survival were monitored until endpoint.

385 Open field analysis with 15 minutes free locomotion was completed at P18, P38, P55 and
386 P75 using SMART v3 software (Harvard Panlab). At endpoint, tissues were collected by snap-
387 freezing or fixing in 4% PFA.

388 **EEG recordings**

389 AAV-F-CIRTS-gRNAluc and AAV-F-CIRTS-gRNA9 treated *Scn1a*$^{+/-}$ mice underwent
390 EEG recordings from P30-P45 using wireless electrocorticogram (ECoG) transmitters (Cat. No.
391 A3048P2-AA-C37-D, single-channel transmitter, Open Source Instruments), as previously
392 described*(42)*.

393 **RNA/DNA extraction, gene expression and VCN**

394 RNA extraction was completed using the PureLink kit (Thermo Fisher Scientfic), DNA
395 extraction was completed using DNeasy Blood & Tissue kit (Qiagen), as previously
396 described*(42)*. The following primers and probes were used to quantify gene expression, titrate
397 AAV vectors and perform vector copy number analyses. *Scn1a;* forward:
398 TCAGAGGGAAGCACAGTAGAC, reverse: TTCCACGCTGATTTGACAGCA, probe:
399 CCAGAAGAAACCCTTGAGCCCGAA (fluorophore: ABY, quencher: QSY, Thermo Fisher

400 Scientific). *Gapdh*; forward: ACGGCAAATTCAACGGCAC, reverse:
401 TAGTGGGGTCTCGCTCCTGG, probe: TTGTCATCAACGGGAAGCCCATCA (fluorophore:
402 VIC, quencher: QSY, Thermo Fisher Scientific). *YTHDF2*; forward:
403 CCTCCATTGGCTTCTCCTATTC, reverse: GTTGCTCAGCTGTCCATAAGA, probe:
404 TTAAGTAGGGCATGGCTGTGTCACC (fluorophore: FAM, quencher: ZEN / Iowa Black™
405 FQ, Integrated DNA Technologies).

406 The same sequence *Gapdh* primers and probe, and *Scn1a* primers were used for ddPCR
407 analysis, but with the *Scn1a* probe fluorophore was adapted from ABY to FAM. 5µL of each
408 cDNA (equivalent to 85 pg) was loaded per reaction with 1X ddPCR Multiplex Supermix (Bio-
409 Rad) and 4 mM DTT. ddPCR analysis was performed using the BioRad QXOne in the UCL
410 NeuroGTx Vector Core Facility. The Facility is supported by the NIHR Great Ormond Street
411 Hospital Biomedical Research Centre. The views expressed are those of the author(s) and not
412 necessarily those of the NHS, the NIHR or the Department of Health.

413 **Immunohistochemistry**

414 40 µm coronal sections cut using a Micron HM 430 freezing microtome (Thermo Fisher
415 Scientific) were analysed using previously published protocols*(42)*. Neuropathological analyses
416 used the following primary antibodies; anti-GFAP (Proteintech 16825-1-AP; 1:2000) and anti-
417 CD68 (BioRad MCA1957; 1:100). Images were acquired using a Leica Microsystems
418 stereoscopic microscope (DM4000), Leica DFC7000T camera and Leica LAX X software (all
419 Leica Microsystems UK). Images were background corrected using FIJI (ImageJ) and
420 thresholding software (Image-Pro Premier v10; Media Cybernetics) was used to quantify
421 expression.

422

423 **RNA-seq**

424 Total RNA was extracted from the cortex of *Scn1a*$^{+/+}$ and *Scn1a*$^{+/-}$ P50 mice that were
425 controls, or had been treated with, AAV-F-CIRTS-gRNAluc or AAV-F-CIRTS-gRNA9.

426 Untreated control samples were processed by UCL Genomics using a KAPA mRNA
427 HyperPrep and NextSeq2000 P2 100c configuration with single-end reads at 25M reads/sample.
428 N=8 mice per genotype were submitted, but due to a pooling error, *Scn1a*$^{+/+}$ Untreated_5 could
429 not be included in the analysis.

430 AAV-CIRTS-treated samples (n=4 per group) were processed by Azenta Life Sciences
431 using Illumina NovaSeq with paired-end reads in 2x150 bp configuration. Trimmomatic v.0.36
432 was used to trim sequence reads to remove adapter sequences before reads were mapped to *Mus*
433 *musculus* GRCm38 reference genome using the STAR aligner v.2.5.2b. Unique gene counts
434 were extracted using featureCounts (Subread package v.1.5.2).

435 Both RNA-seq analyses then used DESeq2*(49)* to determine differential gene expression
436 analysis. Untreated samples were subjected to an absolute Log2 fold change > 0.7, whilst AAV-
437 CIRTS comparisons used an absolute Log2 fold change > 1. In both analyses, genes with an
438 adjusted P value < 0.05 were called differentially expressed genes. A gene ontology analysis was
439 performed on the statistically significant set of genes by implementing enrichGO and
440 clusterProfiler R packages*(50)* to cluster the set of genes based on their molecular function and
441 determine their statistical significance.

442 **Statistical analyses**

443 GraphPad Prism (version 10.3.1, Boston) was used for statistical analyses. All continuous
444 variables are presented as mean±SD in graphs. *In vitro* data were analysed using an unpaired,

445 two-tailed t-test for luciferase assay or one-way ANOVA with Dunnett's multiple comparisons
446 for gRNA screening. Survival was determined using a Log-rank (Mantel-Cox) test. Weights
447 were initially screened for differences with one-way ANOVA with Dunnett's multiple
448 comparisons for group-group comparisons and a mixed-effect analysis was completed with
449 analysis at each individual timepoint. Groups were excluded in mixed-effect analyses from the
450 timepoint that only a single mouse remained. Open field was analysed using two-way ANOVA
451 with Dunnett's multiple comparisons. Racine scaling of febrile seizures were contingency
452 analysed with Fisher's exact test. A mixed-effects analysis was used to compare overall EEG
453 seizure burden, with either Mann-Whitney or unpaired, two-tailed t-test for individual seizure
454 readouts. One-way and two-way ANOVAs were used to analyse all molecular data.

455 **Supplementary Materials**

456 PDF file includes;

457 Fig S1 to S9 supplementary figures

458

459 **REFERENCES**

460 1. E. Chilcott, J. A. Díaz, C. Bertram, M. Berti, R. Karda, Genetic therapeutic advancements for Dravet Syndrome.
461 *Epilepsy & Behavior* **132**, 108741 (2022).

462 2. A. Strzelczyk, L. Lagae, J. Wilmshurst, A. Brunklaus, P. Striano, F. Rosenow, S. Schubert-Bast, Dravet
463 syndrome: a systematic literature review of the illness burden. *Epilepsia Open* (2023).

464 3. A. Brunklaus, S. M. Zuberi, Dravet syndrome—From epileptic encephalopathy to channelopathy. *Epilepsia* **55**,
465 979–984 (2014).

466 4. M. Wolff, C. Cassé-Perrot, C. Dravet, Severe myoclonic epilepsy of infants (Dravet syndrome): natural history
467 and neuropsychological findings. *Epilepsia* **47 Suppl 2**, 45–48 (2006).

468 5. A. Brunklaus, E. Pérez-Palma, I. Ghanty, J. Xinge, E. Brilstra, B. Ceulemans, N. Chemaly, I. de Lange, C.
469 Depienne, R. Guerrini, D. Mei, R. S. Møller, R. Nabbout, B. M. Regan, A. L. Schneider, I. E. Scheffer, A.-S.
470 Schoonjans, J. D. Symonds, S. Weckhuysen, M. W. Kattan, S. M. Zuberi, D. Lal, Development and Validation of a
471 Prediction Model for Early Diagnosis of SCN1A-Related Epilepsies. *Neurology* **98**, e1163–e1174 (2022).

472 6. S. Gataullina, O. Dulac, From genotype to phenotype in Dravet disease. *Seizure* **44**, 58–64 (2017).

473 7. W. R. J. Whitaker, R. L. M. Faull, H. J. Waldvogel, C. J. Plumpton, P. C. Emson, J. J. Clare, Comparative
474 distribution of voltage-gated sodium channel proteins in human brain. *Molecular Brain Research* **88**, 37–53 (2001).

475 8. A. T. Berg, K. Coffman, D. Gaebler-Spira, Dysautonomia and functional impairment in rare developmental and
476 epileptic encephalopathies: the other nervous system. *Developmental Medicine & Child Neurology* **63**, 1433–1440
477 (2021).

478 9. F. Kalume, R. E. Westenbroek, C. S. Cheah, F. H. Yu, J. C. Oakley, T. Scheuer, W. A. Catterall, Sudden
479 unexpected death in a mouse model of Dravet syndrome. *J Clin Invest* **123**, 1798–1808 (2013).

480 10. S. Mishra, V. Reznikov, V. A. Maltsev, N. A. Undrovinas, H. N. Sabbah, A. Undrovinas, Contribution of
481 sodium channel neuronal isoform Nav1.1 to late sodium current in ventricular myocytes from failing hearts. *The*
482 *Journal of Physiology* **593**, 1409–1427 (2015).

483 11. D. S. Auerbach, J. Jones, B. C. Clawson, J. Offord, G. M. Lenk, I. Ogiwara, K. Yamakawa, M. H. Meisler, J. M.
484 Parent, L. L. Isom, Altered Cardiac Electrophysiology and SUDEP in a Model of Dravet Syndrome. *PLOS ONE* **8**,
485 e77843 (2013).

486 12. A. Strzelczyk, S. Schubert-Bast, A Practical Guide to the Treatment of Dravet Syndrome with Anti-Seizure
487 Medication. *CNS Drugs* **36**, 217–237 (2022).

488 13. G. Massaro, C. N. Z. Mattar, A. M. S. Wong, E. Sirka, S. M. K. Buckley, B. R. Herbert, S. Karlsson, D. P.
489 Perocheau, D. Burke, S. Heales, A. Richard-Londt, S. Brandner, M. Huebecker, D. A. Priestman, F. M. Platt, K.
490 Mills, A. Biswas, J. D. Cooper, J. K. Y. Chan, S. H. Cheng, S. N. Waddington, A. A. Rahim, Fetal gene therapy for
491 neurodegenerative disease of infants. *Nature Medicine* (2018), doi:10.1038/s41591-018-0106-7.

492 14. J. Ng, S. Barral, C. de la Fuente Barrigon, G. Lignani, F. A. Erdem, R. Wallings, R. Privolizzi, G. Rossignoli, H.
493 Alrashidi, S. Heasman, E. Meyer, A. Ngoh, S. Pope, R. Karda, D. Perocheau, J. Baruteau, N. Suff, J. A. Diaz, S.
494 Schorge, J. Vowles, L. R. Marshall, S. A. Cowley, S. Sucic, M. Freissmuth, J. R. Counsell, R. Wade-Martins, S. J.
495 R. Heales, A. A. Rahim, M. Bencze, S. N. Waddington, M. A. Kurian, Gene therapy restores dopamine transporter
496 expression and ameliorates pathology in iPSC and mouse models of infantile parkinsonism. *Science Translational*
497 *Medicine* **13**, 1–13 (2021).

498 15. J. R. Mendell, S. Al-Zaidy, R. Shell, W. D. Arnold, L. R. Rodino-Klapac, T. W. Prior, L. Lowes, L. Alfano, K.
499 Berry, K. Church, J. T. Kissel, S. Nagendran, J. L'Italien, D. M. Sproule, C. Wells, J. A. Cardenas, M. D. Heitzer,
500 A. Kaspar, S. Corcoran, L. Braun, S. Likhite, C. Miranda, K. Meyer, K. D. Foust, A. H. M. Burghes, B. K. Kaspar,
501 Single-Dose Gene-Replacement Therapy for Spinal Muscular Atrophy. *New England Journal of Medicine* **377**,
502 1713–1722 (2017).

503 16. K. A. Strauss, M. A. Farrar, F. Muntoni, K. Saito, J. R. Mendell, L. Servais, H. J. McMillan, R. S. Finkel, K. J.
504 Swoboda, J. M. Kwon, C. M. Zaidman, C. A. Chiriboga, S. T. Iannaccone, J. M. Krueger, J. A. Parsons, P. B. Shieh,
505 S. Kavanagh, S. Tauscher-Wisniewski, B. E. McGill, T. A. Macek, Onasemnogene abeparvovec for presymptomatic
506 infants with two copies of SMN2 at risk for spinal muscular atrophy type 1: the Phase III SPR1NT trial. *Nat Med* **28**,
507 1381–1389 (2022).

508 17. D. Chand, F. Mohr, H. McMillan, F. F. Tukov, K. Montgomery, A. Kleyn, R. Sun, S. Tauscher-Wisniewski, P.
509 Kaufmann, G. Kullak-Ublick, Hepatotoxicity following administration of onasemnogene abeparvovec (AVXS-101)
510 for the treatment of spinal muscular atrophy. *Journal of Hepatology* **74**, 560–566 (2021).

511 18. K. S. Hanlon, J. C. Meltzer, T. Buzhdygan, M. J. Cheng, M. Sena-Esteves, R. E. Bennett, T. P. Sullivan, R.
512 Razmpour, Y. Gong, C. Ng, J. Nammour, D. Maiz, S. Dujardin, S. H. Ramirez, E. Hudry, C. A. Maguire, Selection
513 of an Efficient AAV Vector for Robust CNS Transgene Expression. *Molecular Therapy - Methods and Clinical*
514 *Development* **15**, 320–332 (2019).

515 19. A. Beharry, Y. Gong, J. C. Kim, K. S. Hanlon, J. Nammour, K. Hieber, F. Eichler, M. Cheng, A. Stemmer-
516 Rachamimov, K. M. Stankovic, D. B. Welling, C. Ng, C. A. Maguire, The AAV9 Variant Capsid AAV-F Mediates
517 Widespread Transgene Expression in Nonhuman Primate Spinal Cord After Intrathecal Administration. *Hum Gene*
518 *Ther* **33**, 61–75 (2022).

519 20. L. E. Burbano, M. Li, N. Jancovski, P. Jafar-Nejad, K. Richards, A. Sedo, A. Soriano, B. Rollo, L. Jia, E.
520 Gazina, S. Piltz, F. Adikusuma, P. Q. Thomas, F. Rigo, C. A. Reid, S. Maljevic, S. Petrou, Antisense
521 oligonucleotide therapy for KCNT1 encephalopathy, 2020.11.12.379164 (2020).

522 21. Z. Han, C. Chen, A. Christiansen, S. Ji, Q. Lin, C. Anumonwo, C. Liu, S. C. Leiser, I. Aznarez, G. Liau, L. L.
523 Isom, *Antisense oligonucleotides increase Scn1a expression and reduce seizures and SUDEP incidence in a mouse*
524 *model of Dravet syndrome* (2020; http://stm.sciencemag.org/), p. 6100.

525 22. D. W. Morgens, M. Wainberg, E. A. Boyle, O. Ursu, C. L. Araya, C. K. Tsui, M. S. Haney, G. T. Hess, K. Han,
526 E. E. Jeng, A. Li, M. P. Snyder, W. J. Greenleaf, A. Kundaje, M. C. Bassik, Genome-scale measurement of off-
527 target activity using Cas9 toxicity in high-throughput screens. *Nat Commun* **8**, 15178 (2017).

528 23. S. Rauch, E. He, M. Srienc, H. Zhou, Z. Zhang, B. C. Dickinson, Programmable RNA-Guided RNA Effector
529 Proteins Built from Human Parts. *Cell* **178**, 122-134.e12 (2019).

530 24. S. Rauch, K. A. Jones, B. Dickinson, Small Molecule-Inducible RNA-Targeting Systems for Temporal Control
531 of RNA Regulation in Vivo (2020), doi:10.26434/chemrxiv.11673711.v1.

532 25. S. U. Madugalle, W.-S. Liau, Q. Zhao, X. Li, H. Gong, P. R. Marshall, A. Periyakaruppiah, E. L. Zajaczkowski,
533 L. J. Leighton, H. Ren, M. R. B. Musgrove, J. W. A. Davies, G. Kim, S. Rauch, C. He, B. C. Dickinson, B.
534 Fulopova, L. N. Fletcher, S. R. Williams, R. C. Spitale, T. W. Bredy, Synapse-Enriched m6A-Modified Malat1
535 Interacts with the Novel m6A Reader, DPYSL2, and Is Required for Fear-Extinction Memory. *J. Neurosci.* **43**,
536 7084–7100 (2023).

537 26. J. Hsiao, T. Y. Yuan, M. S. Tsai, C. Y. Lu, Y. C. Lin, M. L. Lee, S. W. Lin, F. C. Chang, H. Liu Pimentel, C.
538 Olive, C. Coito, G. Shen, M. Young, T. Thorne, M. Lawrence, M. Magistri, M. A. Faghihi, O. Khorkova, C.
539 Wahlestedt, Upregulation of Haploinsufficient Gene Expression in the Brain by Targeting a Long Non-coding RNA
540 Improves Seizure Phenotype in a Model of Dravet Syndrome. *EBioMedicine* **9**, 257–277 (2016).

541 27. A. R. Miller, N. A. Hawkins, C. E. Mccollom, J. A. Kearney, Mapping genetic modifiers of survival in a mouse
542 model of Dravet syndrome. *Genes, Brain and Behavior* **13**, 163–172 (2014).

543 28. A. M. Mistry, C. H. Thompson, A. R. Miller, C. G. Vanoye, A. L. George,, J. A. Kearney, Strain- and age-
544 dependent hippocampal neuron sodium currents correlate with epilepsy severity in Dravet syndrome mice.
545 *Neurobiology of Disease* **65**, 1–11 (2014).

546 29. A. Tanenhaus, T. Stowe, A. Young, J. McLaughlin, R. Aeran, I. W. Lin, J. Li, R. Hosur, M. Chen, J. Leedy, T.
547 Chou, S. Pillay, M. C. Vila, J. A. Kearney, M. Moorhead, A. Belle, S. Tagliatela, Cell-Selective Adeno-Associated
548 Virus-Mediated SCN1A Gene Regulation Therapy Rescues Mortality and Seizure Phenotypes in a Dravet Syndrome
549 Mouse Model and Is Well Tolerated in Nonhuman Primates. *Hum Gene Ther* **33**, 579–597 (2022).

550 30. J. Van Erum, D. Van Dam, P. P. De Deyn, PTZ-induced seizures in mice require a revised Racine scale.
551 *Epilepsy & Behavior* **95**, 51–55 (2019).

552 31. K. S. Hanlon, J. C. Meltzer, T. Buzhdygan, M. J. Cheng, M. Sena-Esteves, R. E. Bennett, T. P. Sullivan, R.
553 Razmpour, Y. Gong, C. Ng, J. Nammour, D. Maiz, S. Dujardin, S. H. Ramirez, E. Hudry, C. A. Maguire, Selection
554 of an Efficient AAV Vector for Robust CNS Transgene Expression. *Mol Ther Methods Clin Dev* **15**, 320–332
555 (2019).

556 32. A. Brunklaus, T. Brünger, T. Feng, C. Fons, A. Lehikoinen, E. Panagiotakaki, M.-A. Vintan, J. Symonds, J.
557 Andrew, A. Arzimanoglou, S. Delima, J. Gallois, D. Hanrahan, G. Lesca, S. MacLeod, D. Marjanovic, A. McTague,
558 N. Nuñez-Enamorado, E. Perez-Palma, M. Scott Perry, K. Pysden, S. J. Russ-Hall, I. E. Scheffer, K. Sully, S. Syrbe,
559 U. Vaher, M. Velayutham, J. Vogt, S. Weiss, E. Wirrell, S. M. Zuberi, D. Lal, R. S. Møller, M. Mantegazza, S.
560 Cestèle, The gain of function SCN1A disorder spectrum: novel epilepsy phenotypes and therapeutic implications.
561 *Brain* **145**, 3816–3831 (2022).

562 33. N. A. Hawkins, L. L. Anderson, T. S. Gertler, L. Laux, A. L. George Jr., J. A. Kearney, Screening of
563 conventional anticonvulsants in a genetic mouse model of epilepsy. *Annals of Clinical and Translational Neurology*
564 **4**, 326–339 (2017).

565 34. J. P. Pandey, P. J. Nietert, A. M. Namboodiri, C. Kimball, P. A. Flume, Roles of immunoglobulin GM and KM
566 allotypes and Fcγ receptor 2 A genotypes in humoral immunity to a conserved microbial polysaccharide in
567 pulmonary diseases. *Genes Immun* **26**, 91–95 (2025).

568 35. R. Li, L. Ma, H. Huang, S. Ou, J. Yuan, T. Xu, X. Yu, X. Liu, J. Yang, Y. Chen, X. Peng, Altered Expression of
569 CXCL13 and CXCR5 in Intractable Temporal Lobe Epilepsy Patients and Pilocarpine-Induced Epileptic Rats.
570 *Neurochem Res* **42**, 526–540 (2017).

571 36. H.-H. Lin, C.-C. Hsiao, C. Pabst, J. Hébert, T. Schöneberg, J. Hamann, in *Advances in Immunology*, G Protein-
572 Coupled Receptors in Immune Response and Regulation. A. K. Shukla, Ed. (Academic Press, 2017), vol. 136, pp.
573 163–201.

574 37. J. K. Mich, J. Ryu, A. D. Wei, B. B. Gore, R. Guo, A. M. Bard, R. A. Martinez, E. M. Luber, J. Liu, Y. M.
575 Bishaw, R. J. Christian, L. M. Oliveira, N. Miranda, J.-M. Ramirez, J. T. Ting, E. S. Lein, B. P. Levi, F. K. Kalume,
576 Interneuron-specific dual-AAV SCN1A gene replacement corrects epileptic phenotypes in mouse models of Dravet
577 syndrome. *Science Translational Medicine* **17**, eadn5603 (2025).

578 38. A. Ricobaraza, M. Bunuales, M. Gonzalez-Aparicio, S. Fadila, M. Rubinstein, I. Vides-Urrestarazu, J. Banderas,
579 N. Sola-Sevilla, R. Sanchez-Carpintero, J. L. Lanciego, E. Roda, A. Honrubia, P. Arnaiz, R. Hernandez-Alcoceba,
580 Preferential expression of SCN1A in GABAergic neurons improves survival and epileptic phenotype in a mouse
581 model of Dravet syndrome. *J Mol Med* **101**, 1587–1601 (2023).

582 39. G. Colasante, G. Lignani, S. Brusco, C. Di Berardino, J. Carpenter, S. Giannelli, N. Valassina, S. Bido, R. Ricci,
583 V. Castoldi, S. Marenna, T. Church, L. Massimino, G. Morabito, F. Benfenati, S. Schorge, L. Leocani, D. M.
584 Kullmann, V. Broccoli, dCas9-Based Scn1a Gene Activation Restores Inhibitory Interneuron Excitability and
585 Attenuates Seizures in Dravet Syndrome Mice. *Molecular Therapy* **28**, 235–253 (2020).

586 40. T. Yamagata, M. Raveau, K. Kobayashi, H. Miyamoto, T. Tatsukawa, I. Ogiwara, S. Itohara, T. K. Hensch, K.
587 Yamakawa, CRISPR/dCas9-based Scn1a gene activation in inhibitory neurons ameliorates epileptic and behavioral
588 phenotypes of Dravet syndrome model mice. *Neurobiology of Disease* **141**, 104954 (2020).

589 41. M. F. Schneider, M. Vogt, J. Scheuermann, V. Müller, A. H. L. Fischer-Hentrich, T. Kremer, S. Lugert, F.
590 Metzger, M. Kudernatsch, G. Kluger, T. Hartlieb, S. Noachtar, C. Vollmar, M. Kunz, J. C. Tonn, R. Coras, I.
591 Blümcke, C. Pace, F. Heinen, C. Klein, H. Potschka, I. Borggraefe, Brain expression profiles of two SCN1A
592 antisense RNAs in children and adolescents with epilepsy. *Transl Neurosci* **15**, 20220330 (2024).

593 42. J. Antinao Diaz, E. Chilcott, A. Almacellas Barbanoj, A. Keegan, A. McTague, J. H. Cross, S. Schorge, G.
594 Lignani, S. N. Waddington, R. Karda, AAV9-mediated targeting of natural antisense transcript as a novel treatment
595 for Dravet Syndrome. *bioRxiv* , 2024.09.27.615323 (2024).

596 43. Z. Han, C. Chen, A. Christiansen, S. Ji, Q. Lin, C. Anumonwo, C. Liu, S. C. Leiser, Meena, I. Aznarez, G. Liau,
597 L. L. Isom, Antisense oligonucleotides increase *Scn1a* expression and reduce seizures and SUDEP incidence in a
598 mouse model of Dravet syndrome. *Sci. Transl. Med.* **12**, eaaz6100 (2020).

599 44. Encoded Therapeutics Announces US IND Clearance and Australian CTA Approval for Dravet Syndrome Gene
600 Therapy Candidate ETX101*Encoded Therapeutics, Inc.* (available at https://encoded.com/press-releases/encoded-
601 therapeutics-announces-us-ind-clearance-and-australian-cta-approval-for-dravet-syndrome-gene-therapy-candidate-
602 etx101/).

603 45. Z. Liu, O. Chen, J. B. J. Wall, M. Zheng, Y. Zhou, L. Wang, H. Ruth Vaseghi, L. Qian, J. Liu, Systematic
604 comparison of 2A peptides for cloning multi-genes in a polycistronic vector. *Sci Rep* **7**, 2193 (2017).

605 46. X. Xiao, J. Li, R. J. Samulski, Production of high-titer recombinant adeno-associated virus vectors in the absence
606 of helper adenovirus. *J Virol* **72**, 2224–2232 (1998).

607 47. J.-Y. Kim, S. D. Grunke, Y. Levites, T. E. Golde, J. L. Jankowsky, Intracerebroventricular Viral Injection of the
608 Neonatal Mouse Brain for Persistent and Widespread Neuronal Transduction. *Journal of Visualized Experiments*
609 *(JoVE)* , e51863 (2014).

610 48. S. E. Gombash Lampe, B. K. Kaspar, K. D. Foust, Intravenous Injections in Neonatal Mice. *J Vis Exp* , 52037
611 (2014).

612 49. M. I. Love, W. Huber, S. Anders, Moderated estimation of fold change and dispersion for RNA-seq data with
613 DESeq2. *Genome Biology* **15**, 550 (2014).

614 50. T. Wu, E. Hu, S. Xu, M. Chen, P. Guo, Z. Dai, T. Feng, L. Zhou, W. Tang, L. Zhan, X. Fu, S. Liu, X. Bo, G.
615 Yu, clusterProfiler 4.0: A universal enrichment tool for interpreting omics data. *The Innovation* **2**, 100141 (2021).

616

617 **Acknowledgments:** We would like to thank A. Rahim and J. Baruteau for the use of their Home
618 Office PPL. We would like to thank, R.Towns, M. Bandol, N. Foster, N. Marzouki and the staff
619 from Biological Services for their help with maintenance of the DS colony at University College
620 London. Figures 1A and 2A were created in BioRender. Antinao Diaz, J. (2025)
621 https://BioRender.com/k81r069.

622

623 **Funding:** This work was supported by Great Ormond Street Hospital Children Charity and
624 Dravet Syndrome UK Charity (V4720 and V4919 to R.K), Medical Research Council
625 Development Pathway Funding Scheme (MR/Z505201/1 to R.K), LifeArc (P2020-
626 0008 and P2023-0011 to R.K), Therapeutic Acceleration Support (TAS), UCL (to R.K),
627 GOSH/Spark Research Grant V4019 (to G.L.), Medical Research Council Programme Grant
628 (MR/V034758/1 to G.L. and S.S.), Epilepsy Research UK Emerging Leader Fellowship (F1701
629 to G.L.), Medical Research Council New Investigator Project Grant (MR/S011005/1 to G.L.).

630

631 **Author contributions:** Conceptualization: R.K and S.N.W. Methodology: R.K, M.M and
632 E.M.C. Investigation: R.K, E.M.C, J.F.A.D, A.K, Z.W, V.F, A.A.B, G.L. Visualization: R.K and
633 E.M.C. Funding acquisition: R.K, S.S, M.M, S.N.W and G.L. Project administration: R.K.
634 Writing – original draft: R.K and E.M.C. Writing – review & editing: all authors.

635 **Competing interests:** RK, EMC, MM are co-inventors on patent application "Therapy for
636 Dravet Syndrome". RK, SS & SNW have consultancy agreements with Rocket Pharma. G.L. and
637 S.S. have equity in a company that aims to bring epilepsy gene therapy to the clinic.

638

639 **Data and materials availability:** All data associated with this study are present in the paper in
640 Supplementary Material. Requests for data should be addressed to R.K.

641

642 **Figures**

643 **Fig. 1**. **Novel gRNAs increase in endogenous *Scn1a in vitro*.** (A) Schematic illustrating
644 mechanism of action of CIRTS to increase endogenous *Scn1a* expression through targeting of
645 the lncRNA. (B) Schematic diagram of the AAV-CIRTS-gRNA construct. (C) 4 novel AAV-
646 CIRTS-gRNA constructs significantly increased endogenous *Scn1a* mRNA after transient
647 transfection of differentiated mouse Neuro2a cells. The homology of these gRNAs to the human
648 *SCN1ANAT* sequence are indicated on the graph as a %, with gRNAs ranked from least to most
649 homologous. One-way ANOVA with Dunnett's multiple comparisons.

650

651 **Fig. 2. Neonatal AAV-F-CIRTS-gRNA9 RNA editing *in vivo* increases survival of *Scn1a*$^{+/-}$**
652 **DS mice.** *Scn1a*$^{+/-}$ mice were administered either AAV-F-CIRTS-gRNA9 ($7x10^{10}$ vg/pup) or
653 AAV9-CIRTS-gRNA9 ($7x10^{11}$ vg/pup) at P0 by intracerebroventricular (ICV) and intravenous
654 (IV) injection, with PBS-treated *Scn1a*$^{+/-}$ and *Scn1a*$^{+/+}$ littermate controls. (A) Experimental
655 timeline. (B) Kaplan-Meier survival curves of treated mice with percentage survival shown. Log-
656 rank (Mantel-Cox) test. (C) Weights of treated mice. One-way ANOVA with Dunnett's multiple

657 comparison. (D) Total distance read-outs from open field analyses at 4 different timepoints.
658 Two-way ANOVA with Dunnett's multiple comparisons.

659

660 **Fig. 3. Dosage study of AAV-F-CIRTS-gRNA9 in *Scn1a*$^{+/-}$ mice.** AAV-F-CIRTS-gRNA9 was
661 administered at 2 additional doses ($1.75x10^{10}$ and $1.75x10^{11}$ vg/pup) and was compared to the
662 original $7x10^{10}$ vg/pup cohort presented in Fig. 2. (A) Kaplan-Meier survival curves of treated
663 mice with percentage survival shown. Log-rank (Mantel-Cox) test. (B) Weights of treated mice.
664 AAV-F-CIRTS-gRNA9 $1.75x10^{11}$ vg/pup mice were significantly different from *Scn1a*$^{+/-}$ PBS
665 mice at P70 & P80-95 (P=0.0214-0.0451). Mixed-effects analysis with Geisser-Greenhouse
666 correction. (C) Total distance read-outs from open field analyses at 4 different timepoints. Two-
667 way ANOVA with Dunnett's multiple comparisons.

668

669 **Fig. 4. Reduction of seizure burden following AAV-F-CIRTS-gRNA9 treatment.** (A) Febrile
670 seizure probability curves. (B) Severity of observed seizures ranked by Racine scale. Fisher's
671 exact test. (C) Heatmap with coloured squares indicating seizure activity, monitored by EEG.
672 Crosses indicate the death of an animal during EEG recording. (D) Average seizure duration in
673 mice which presented with seizures, during EEG. Unpaired, two-tailed t-test.

674

675 **Fig. 5. Restoration of *Scn1a* gene expression in the cortex and heart of AAV-F-CIRTS-**
676 **gRNA9 treated *Scn1a*$^{+/-}$ mice.** *Scn1a* gene expression in the (A) cortex and (B) heart between
677 *Scn1a*$^{+/+}$ and *Scn1a*$^{+/-}$ mice (P20-100 tissues) treated with non-targeting AAV-F-CIRTS-
678 gRNAluc vector compared to AAV-F-CIRTS-gRNA9 *Scn1a*$^{+/-}$ mice. One-way ANOVA with

679 Dunnett's multiple comparisons. (C) Vector copy number analysis in P100 cortex, heart and
680 liver. Two-way ANOVA with Tukey's multiple comparisons.

681

682 **Fig. 6. AAV-F-CIRTS-gRNA9 does not lead to toxicity *in vivo*.** (A) Representative brain and
683 liver immunohistochemistry images. Scale bar = 100 μm. (B) Quantification of reactive
684 astrocytes (GFAP immunohistochemistry) in the brain of treated mice; CA1 = CA1 region of the
685 hippocampus, CA3 = CA3 region of the hippocampus, VPM = Ventral posteromedial nucleus of
686 the thalamus. Two-way ANOVA with Šídák's multiple comparisons. (C) Quantification of
687 macrophages (CD68 immunohistochemistry) in the liver of treated mice**.** One-way ANOVA with
688 Dunnett's multiple comparisons.

689

690 **Fig. 7. RNA-seq depicting differential gene expression following AAV-F-CIRTS-gRNA9**
691 **treatment.** *Scn1a*$^{+/-}$ cortical tissue analysed at P50. Comparison of AAV-F-CIRTS-gRNAluc
692 and AAV-F-CIRTS-gRNA9 mice. (A) Volcano plot showing the main differentially expressed
693 genes (DEGs). (B) Heatmap showing top up- and down-regulated genes per comparison,
694 presented as z-score, ranked by P value. Driver gene ontology (GO) term classification of the
695 molecular function of (C) down-regulated DEGs. No molecular function GO terms for up-
696 regulated genes were identified.

697

698 **Fig. S1. *In vitro* validation of AAV-CIRTS machinery.** (A) AAV-CIRTS-gRNAluc
699 significantly down-regulated luciferase expression in HEK293T cells after transient co-

700 transfection with AAV-SFFV-*luciferase*-T2A-*eGFP* plasmid. Luciferase expression normalised
701 to protein concentration within lysate. Unpaired, two-tailed t-test.

702

703 **Fig. S2. Characterisation of untreated *Scn1a*$^{+/-}$ DS mice.** (A) Kaplan-Meier survival curves of
704 untreated mice over 100 days of development with percentage survival shown. Log-rank
705 (Mantel-Cox) test. (B) Weights of untreated mice. (C) Total distance and maximum speed read-
706 outs from open field analyses at 4 different timepoints. Two-way ANOVA with Dunnett's
707 multiple comparisons. (D) Induction of febrile seizures with temperature of seizure onset. (E)
708 *Scn1a* gene expression in 4 brain regions. Two-way ANOVA with Šídák's multiple comparisons
709 within each brain region. (F) Quantification of reactive astrogliosis (GFAP
710 immunohistochemistry) in the brain of untreated mice; CA1 = CA1 region of the hippocampus,
711 CA3 = CA3 region of the hippocampus, VPM = Ventral posteromedial nucleus of the thalamus.

712

713 **Fig. S3. RNA-Seq analysis of untreated *Scn1a*$^{+/-}$ DS mice.** *Scn1a*$^{+/+}$and *Scn1a*$^{+/-}$ cortical tissue
714 analysed at P50. (A) Volcano plot showing the main differentially expressed genes. (B) Heatmap
715 showing top 10 up- and down-regulated genes, presented as z-score, ranked by P value. (C)
716 Confirmation of *Scn1a* down-regulation in *Scn1a*$^{+/-}$ mice with normalised read count, (-
717 0.77Log2FC P=5.85x10^{-6}). (D) Driver gene ontology (GO) term classification of the molecular
718 function of up-regulated DEGs. No molecular function GO terms for down-regulated genes were
719 identified.

720

721 **Fig. S4. Maximum speed of AAV-F/9-CIRTS-gRNA9 mice and survival curve for AAV-F-**
722 **CIRTS-gRNA9.** (A) Open field maximum speed assessment at 4 different timepoints. Two-way
723 ANOVA with Dunnett's multiple comparisons. (B) Kaplan-Meier survival curves of treated mice
724 with percentage survival shown. Log-rank (Mantel-Cox) test.

725

726 **Fig. S5. Neonatal AAV-F/9-CIRTS- gRNA21 treatment.** *Scn1a*$^{+/-}$ mice were administered
727 either AAV-F-CIRTS-gRNA21 at 7x10^{10} vg/pup or AAV-9-CIRTS-gRNA21 at 7x10^{11} vg/pup,
728 with PBS-treated *Scn1a*$^{+/-}$ and *Scn1a*$^{+/+}$ littermate controls. (A) Kaplan-Meier survival curves of
729 treated mice with percentage survival shown. Log-rank (Mantel-Cox) test. (B) Weights of treated
730 mice. AAV-9-CIRTS-gRNA21 was significantly different from *Scn1a*$^{+/-}$ PBS mice at P90 only
731 (P=0.0390), but only female mice were alive in the treatment group at this time (100% female at
732 P100 vs 25% female in *Scn1a*$^{+/-}$ PBS). Mixed-effects analysis with Geisser-Greenhouse
733 correction. (C) Total distance and (D) maximum speed read-outs from open field analyses at 4
734 different timepoints. Two-way ANOVA with Dunnett's multiple comparisons.

735

736 **Fig. S6. Maximum speed of AAV-F-CIRTS-gRNA9 dosage.** 4 different timepoints. Two-way
737 ANOVA with Dunnett's multiple comparisons.

738

739 **Fig. S7. Seizure monitoring in AAV-F-CIRTS-gRNA9 treated DS mice.** (A) Total seizures
740 measured in 15 days. Mann-Whitney test. (B) Average number of seizures per day. Unpaired,
741 two tailed t-test (C) Cumulative seizure duration. Unpaired, two tailed t-test.

742

743 **Fig. S8. *YTHDF2* gene expression analysis.** P100 cortex, heart and liver. Two-way ANOVA
744 with Tukey's multiple comparisons.

745

746 **Fig. S9. AAV-F-CIRTS-gRNA9/luc administration to healthy mice.** *Scn1a*$^{+/+}$ mice were
747 administered either AAV-F-CIRTS-gRNA9 or AAV-F-CIRTS-gRNAluc at the optimum
748 therapeutic dose $7x10^{10}$ vg/pup, or 1 dose higher at $1.75x10^{11}$ vg/pup to assess signs of toxicity,
749 compared to PBS littermates. (A) Kaplan-Meier survival curves of treated mice with percentage
750 survival shown. Log-rank (Mantel-Cox) test. (B) Weights of treated mice. One-way ANOVA
751 with Dunnett's multiple comparison. (C) Total distance and (D) maximum speed read-outs from
752 open field analyses at 4 different timepoints. Two-way ANOVA with Dunnett's multiple
753 comparisons.

Figure 1

A

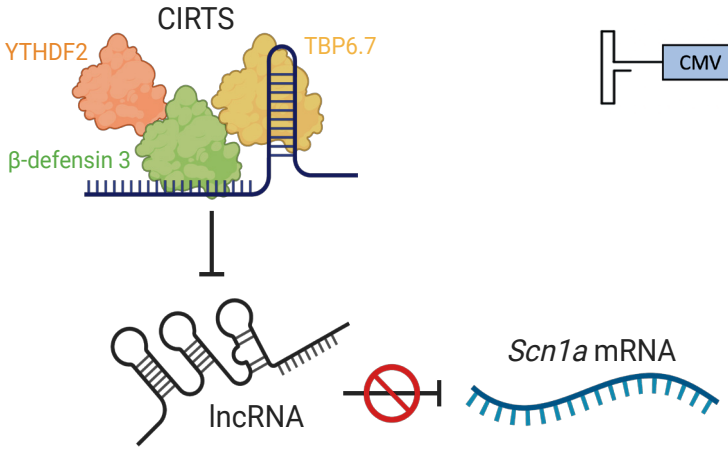
CIRTS
YTHDF2
TBP6.7
β-defensin 3
lncRNA
Scn1a mRNA

B

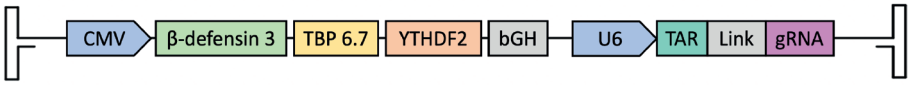
CMV
β-defensin 3
TBP 6.7
YTHDF2
bGH
U6
TAR
Link
gRNA

C

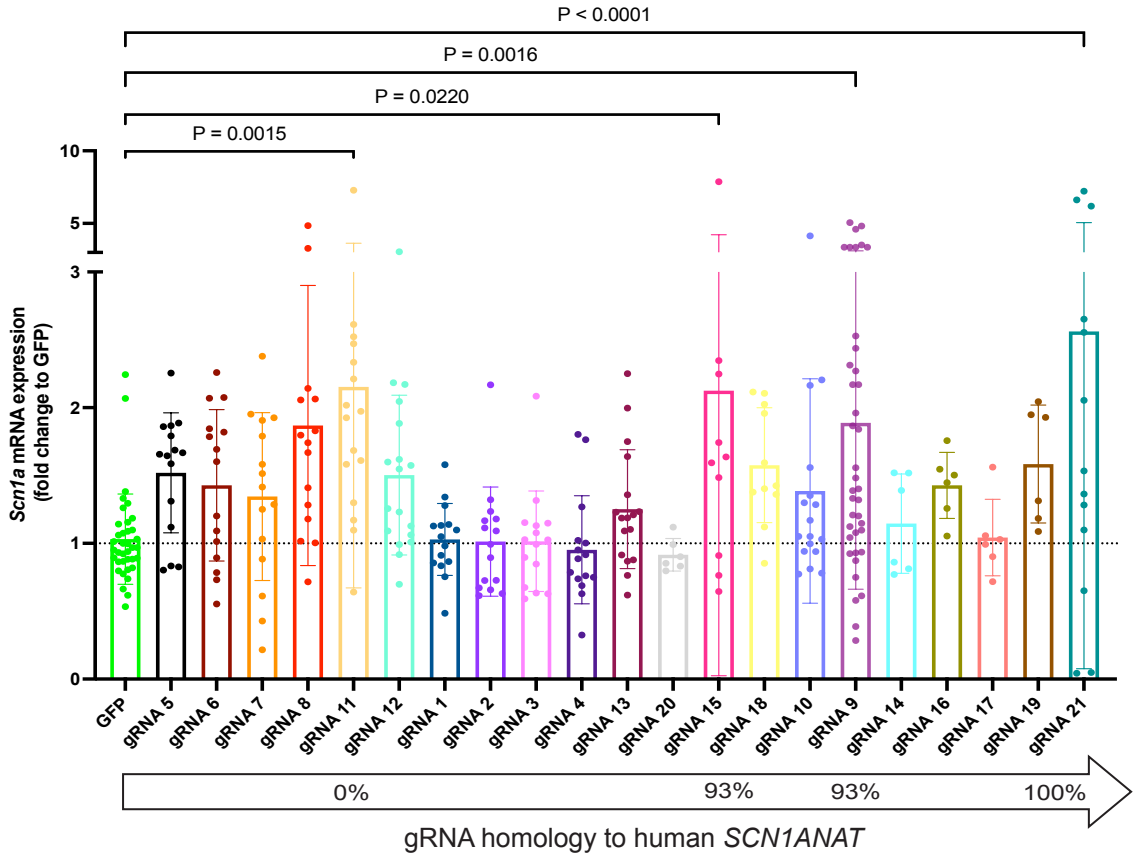
P < 0.0001
P = 0.0016
P = 0.0220
P = 0.0015
Scn1a mRNA expression (fold change to GFP)
GFP
gRNA 5
gRNA 6
gRNA 7
gRNA 8
gRNA 11
gRNA 12
gRNA 1
gRNA 2
gRNA 3
gRNA 4
gRNA 13
gRNA 20
gRNA 15
gRNA 18
gRNA 10
gRNA 9
gRNA 14
gRNA 16
gRNA 17
gRNA 19
gRNA 21
0%
93%
93%
100%
gRNA homology to human SCN1ANAT

Figure 2

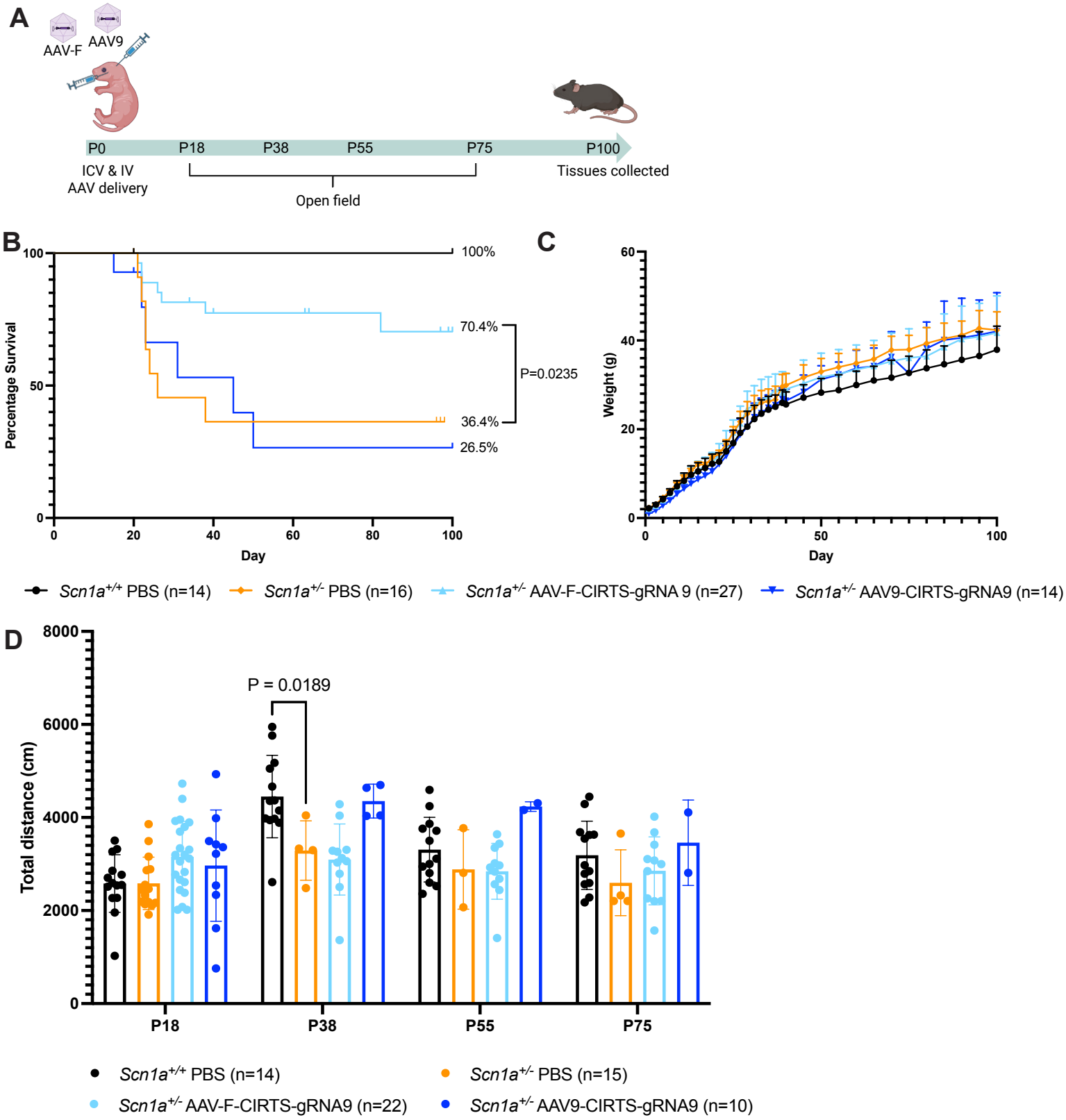
A
AAV-F
AAV9
P0
P18
P38
P55
P75
P100
ICV & IV
AAV delivery
Open field
Tissues collected
B
Percentage Survival
Day
100%
70.4%
36.4%
26.5%
P=0.0235
C
Weight (g)
Day
Scn1a+/+ PBS (n=14)
Scn1a+/- PBS (n=16)
Scn1a+/- AAV-F-CIRTS-gRNA 9 (n=27)
Scn1a+/- AAV9-CIRTS-gRNA9 (n=14)
D
Total distance (cm)
P = 0.0189
P18
P38
P55
P75
Scn1a+/+ PBS (n=14)
Scn1a+/- PBS (n=15)
Scn1a+/- AAV-F-CIRTS-gRNA9 (n=22)
Scn1a+/- AAV9-CIRTS-gRNA9 (n=10)

Figure 3

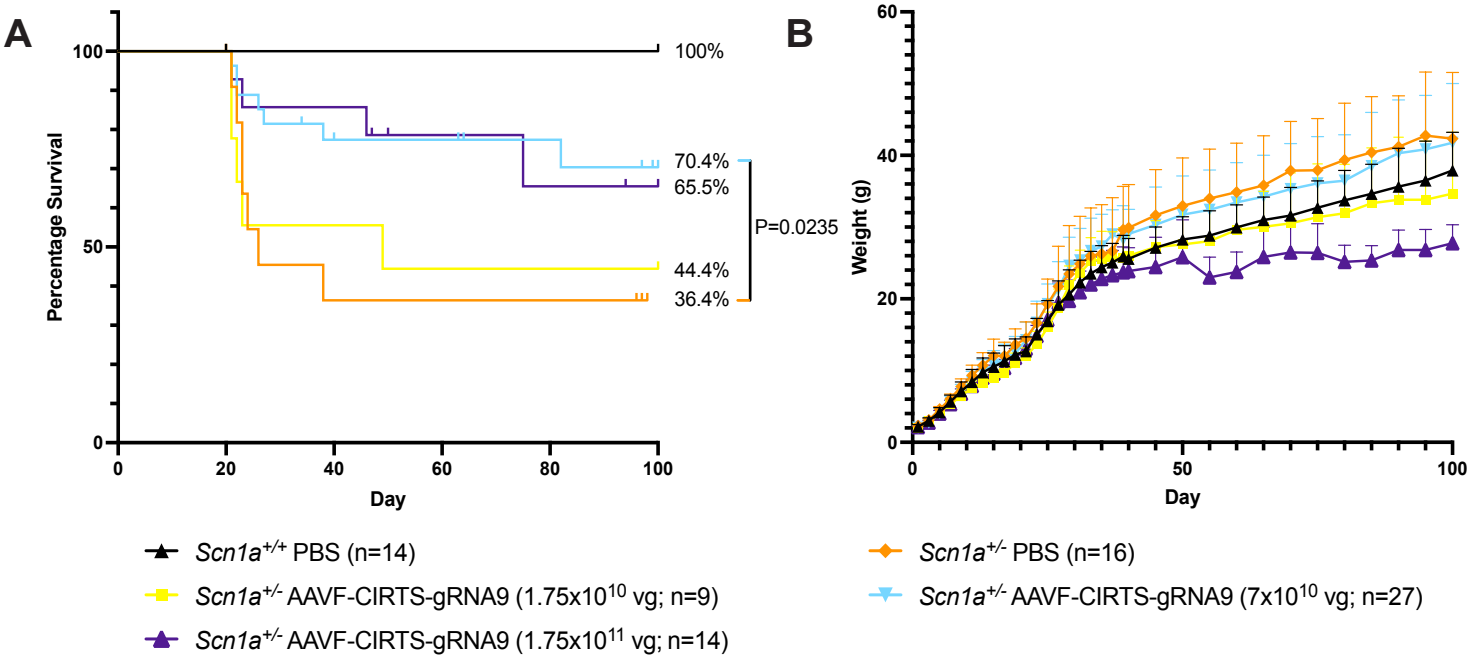
A
Percentage Survival
Day
100%
70.4%
65.5%
44.4%
36.4%
P=0.0235
B
Weight (g)
Day
Scn1a+/+ PBS (n=14)
Scn1a+/- AAVF-CIRTS-gRNA9 (1.75x10^10 vg; n=9)
Scn1a+/- AAVF-CIRTS-gRNA9 (1.75x10^11 vg; n=14)
Scn1a+/- PBS (n=16)
Scn1a+/- AAVF-CIRTS-gRNA9 (7x10^10 vg; n=27)

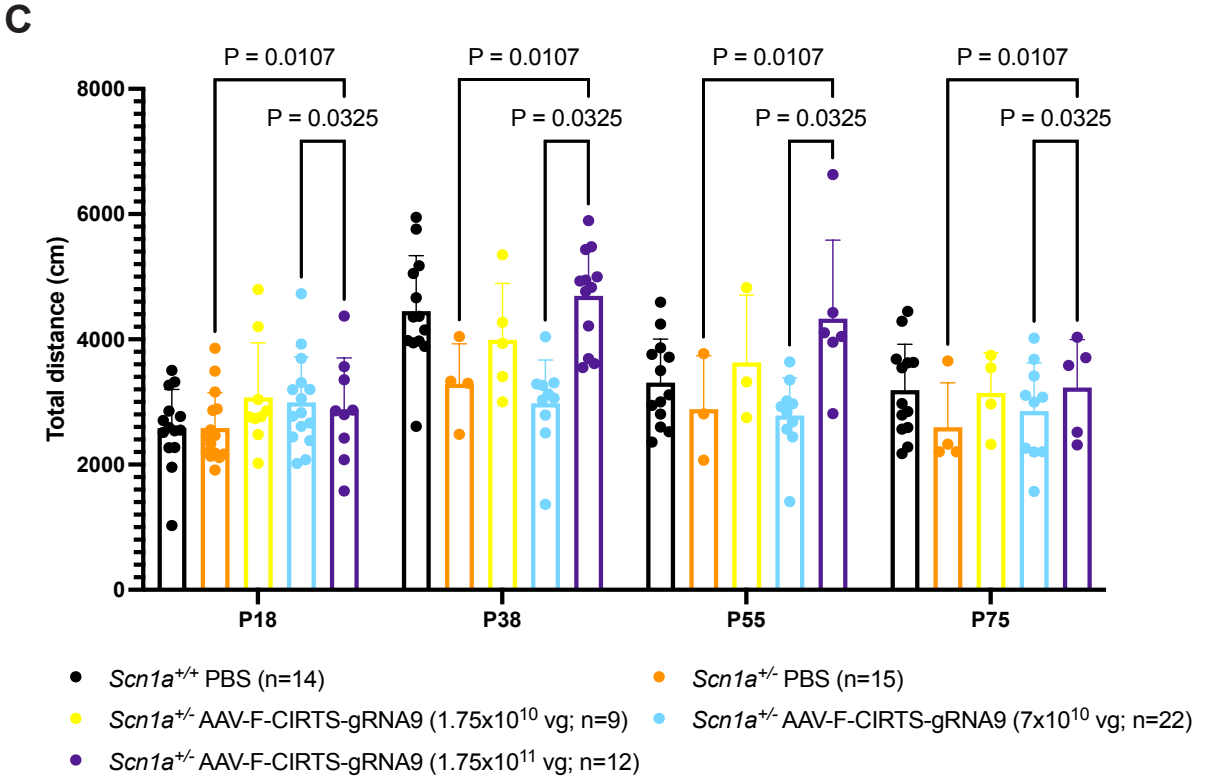
C
Total distance (cm)
P = 0.0107
P = 0.0325
P18
P38
P55
P75
Scn1a+/+ PBS (n=14)
Scn1a+/- PBS (n=15)
Scn1a+/- AAV-F-CIRTS-gRNA9 (1.75x10^10 vg; n=9)
Scn1a+/- AAV-F-CIRTS-gRNA9 (7x10^10 vg; n=22)
Scn1a+/- AAV-F-CIRTS-gRNA9 (1.75x10^11 vg; n=12)

Figure 4

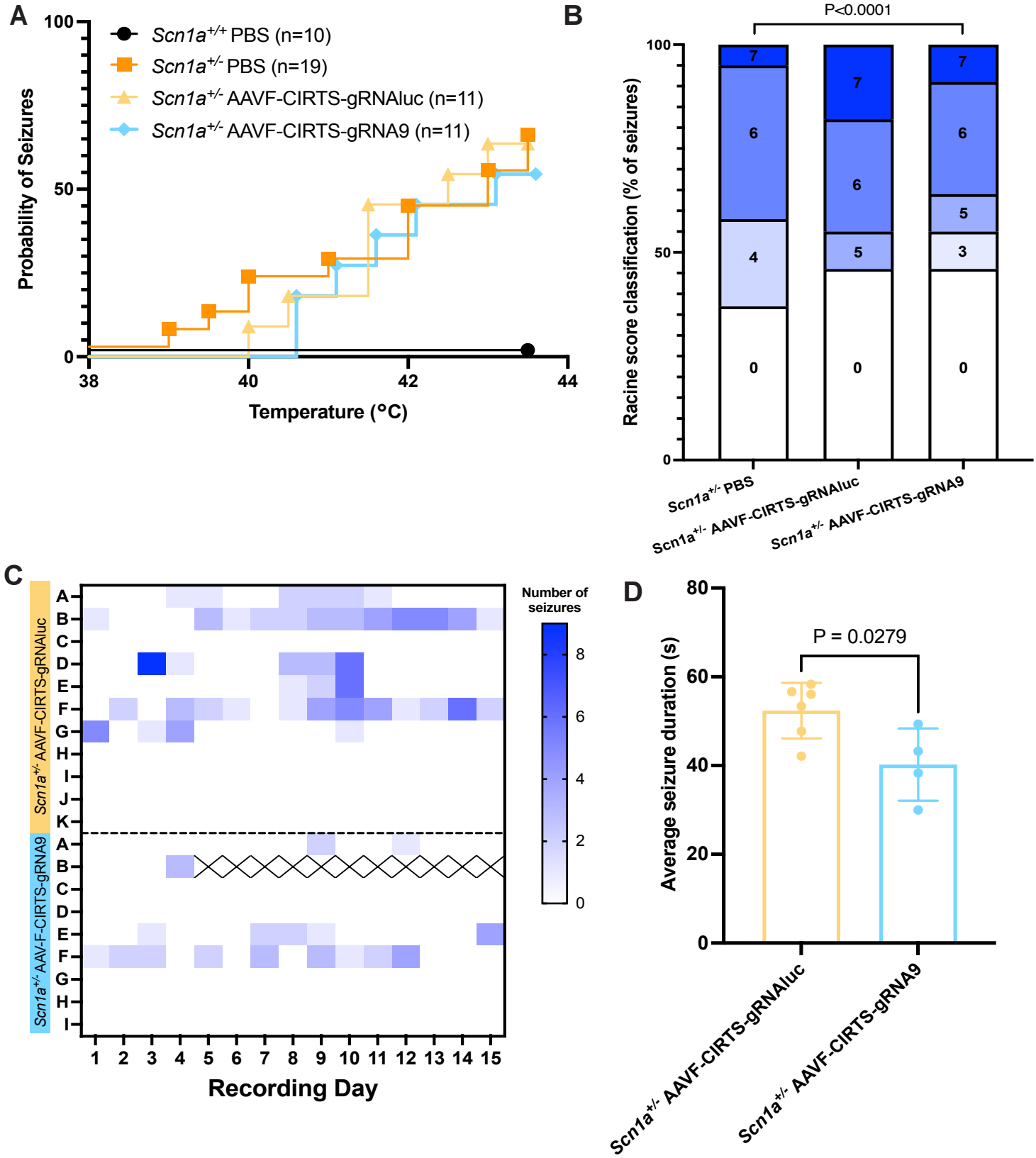
A
Probability of Seizures
Temperature (°C)
Scn1a+/+ PBS (n=10)
Scn1a+/- PBS (n=19)
Scn1a+/- AAVF-CIRTS-gRNAluc (n=11)
Scn1a+/- AAVF-CIRTS-gRNA9 (n=11)
B
Racine score classification (% of seizures)
P<0.0001
P=0.0111
P<0.0001
Scn1a+/- PBS
Scn1a+/- AAVF-CIRTS-gRNAluc
Scn1a+/- AAVF-CIRTS-gRNA9
C
Scn1a+/- AAVF-CIRTS-gRNAluc
Scn1a+/- AAV-F-CIRTS-gRNA9
Number of seizures
Recording Day
D
Average seizure duration (s)
P = 0.0279
Scn1a+/- AAVF-CIRTS-gRNAluc
Scn1a+/- AAVF-CIRTS-gRNA9

Figure 5

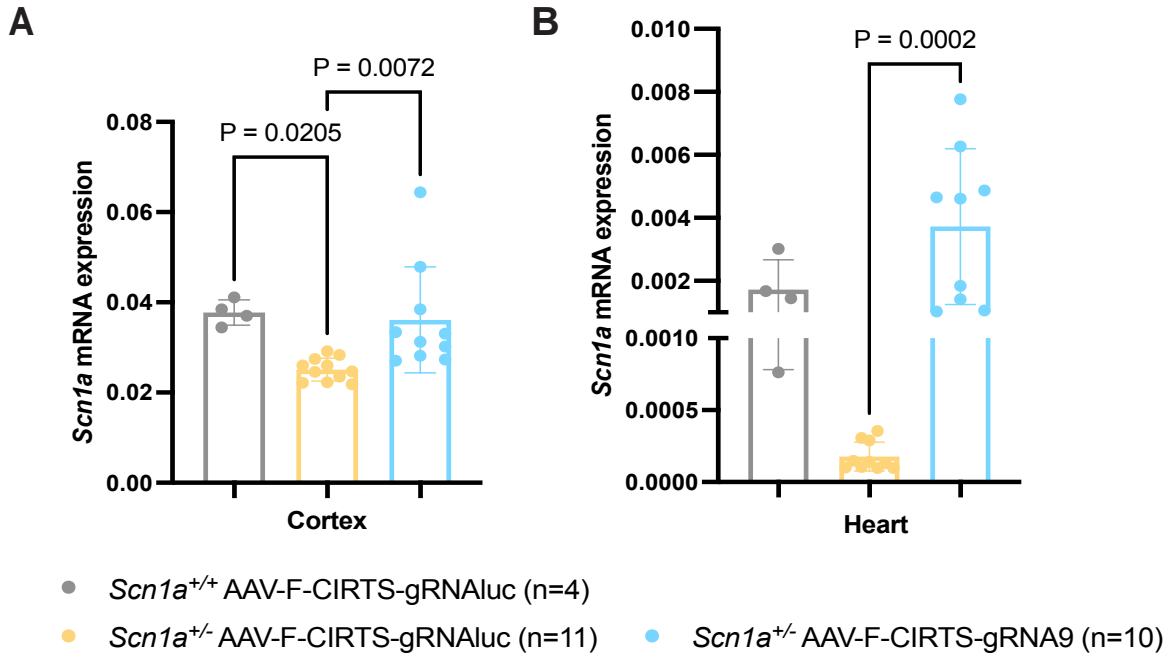
A
B
P = 0.0072
P = 0.0205
P = 0.0002
Scn1a mRNA expression
0.08
0.06
0.04
0.02
0.00
0.010
0.008
0.006
0.004
0.002
0.0010
0.0005
0.0000
Cortex
Heart
Scn1a+/+ AAV-F-CIRTS-gRNAluc (n=4)
Scn1a+/- AAV-F-CIRTS-gRNAluc (n=11)
Scn1a+/- AAV-F-CIRTS-gRNA9 (n=10)

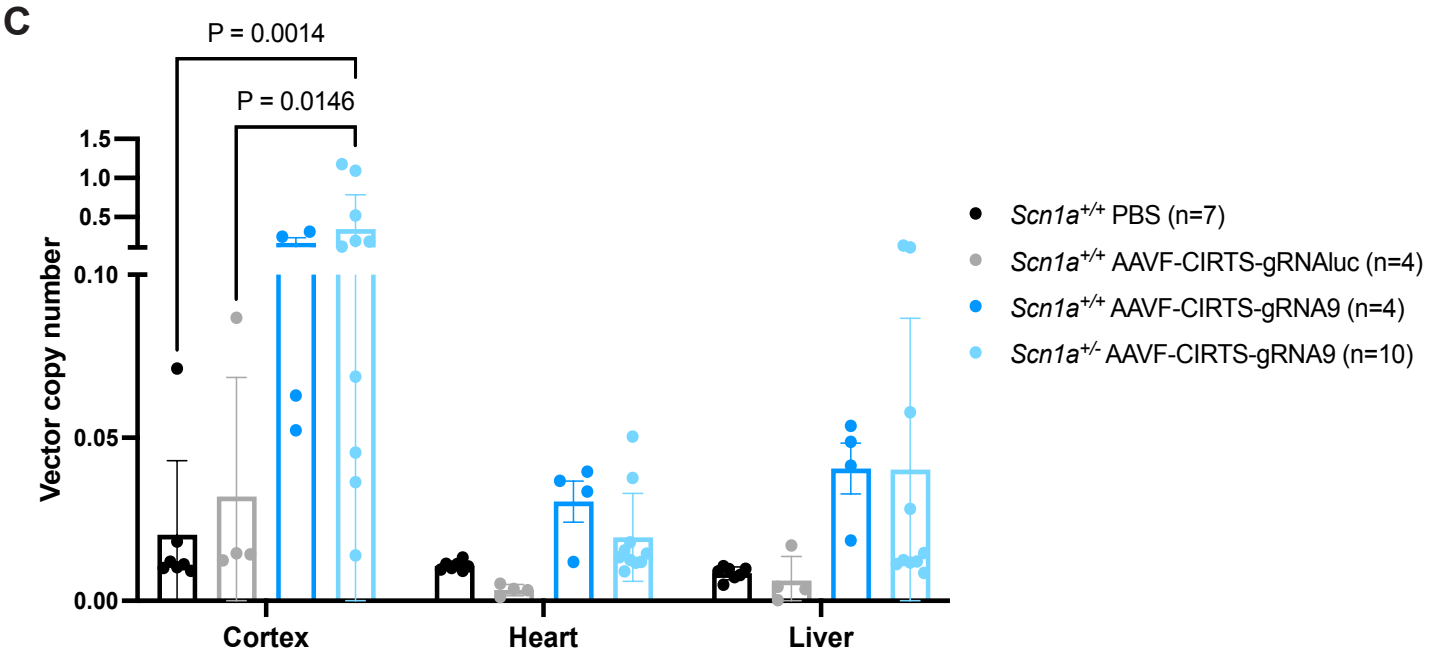
C
P = 0.0014
P = 0.0146
Vector copy number
1.5
1.0
0.5
0.10
0.05
0.00
Cortex
Heart
Liver
Scn1a+/+ PBS (n=7)
Scn1a+/+ AAVF-CIRTS-gRNAluc (n=4)
Scn1a+/+ AAVF-CIRTS-gRNA9 (n=4)
Scn1a+/- AAVF-CIRTS-gRNA9 (n=10)

Figure 6

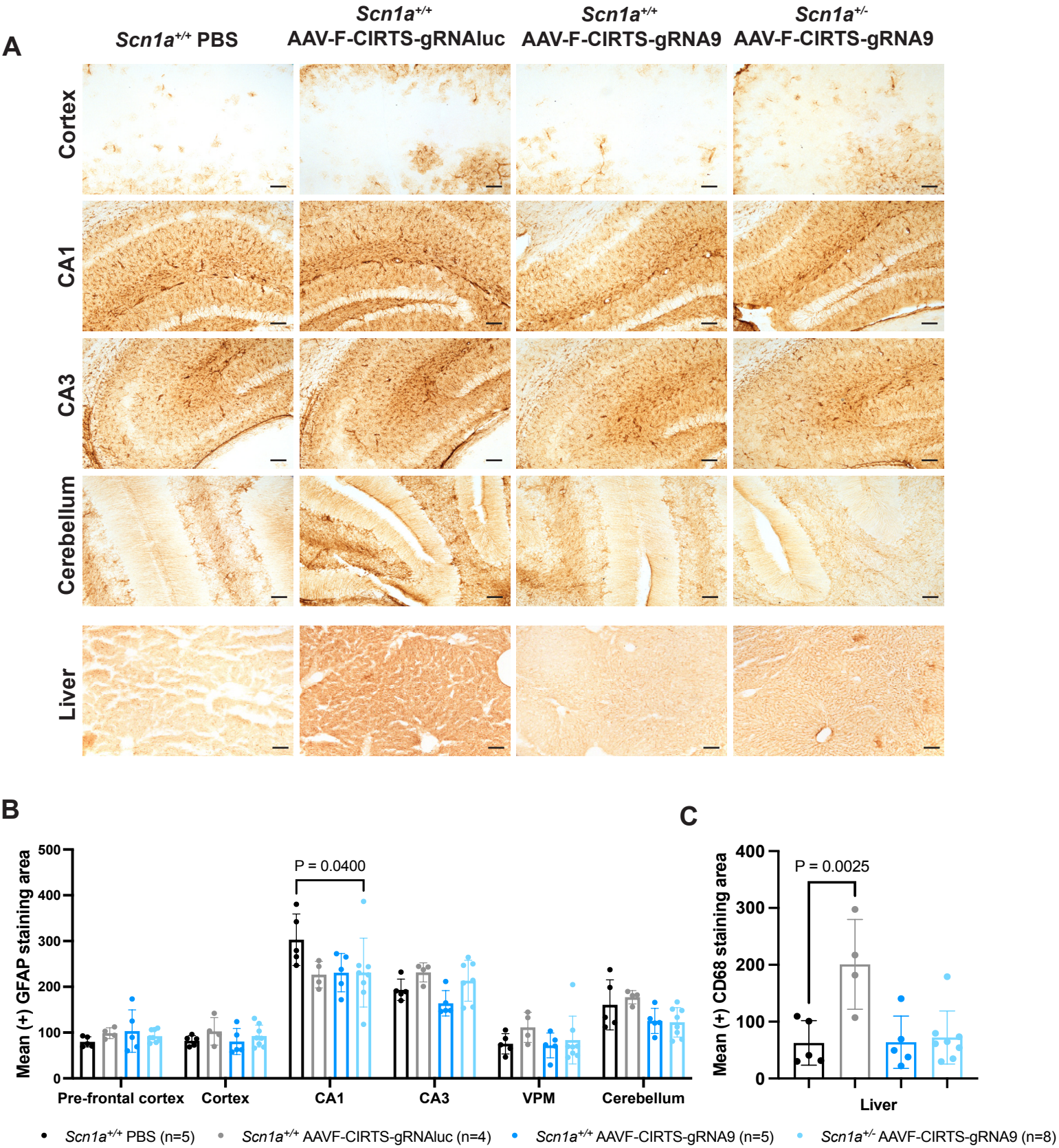
A
Scn1a+/+ PBS
Scn1a+/+ AAV-F-CIRTS-gRNAluc
Scn1a+/+ AAV-F-CIRTS-gRNA9
Scn1a+/- AAV-F-CIRTS-gRNA9
Cortex
CA1
CA3
Cerebellum
Liver
B
Mean (+) GFAP staining area
500
400
300
200
100
0
P = 0.0400
Pre-frontal cortex
Cortex
CA1
CA3
VPM
Cerebellum
C
Mean (+) CD68 staining area
400
300
200
100
0
P = 0.0025
Liver
Scn1a+/+ PBS (n=5)
Scn1a+/+ AAVF-CIRTS-gRNAluc (n=4)
Scn1a+/+ AAVF-CIRTS-gRNA9 (n=5)
Scn1a+/- AAVF-CIRTS-gRNA9 (n=8)

Figure 7

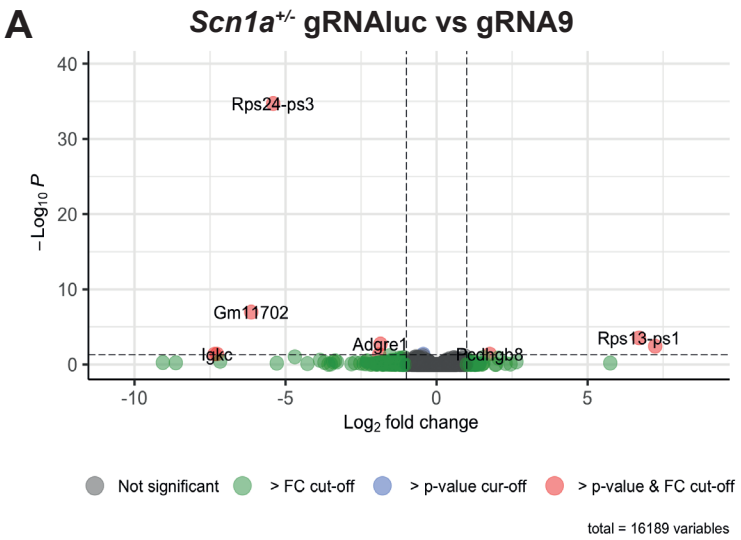
A
Scn1a+/- gRNAluc vs gRNA9
Rps24-ps3
Gm11702
Igkc
Adgre1
Pcdhgb8
Rps13-ps1
−Log10 P
Log2 fold change
Not significant
> FC cut-off
> p-value cur-off
> p-value & FC cut-off
total = 16189 variables

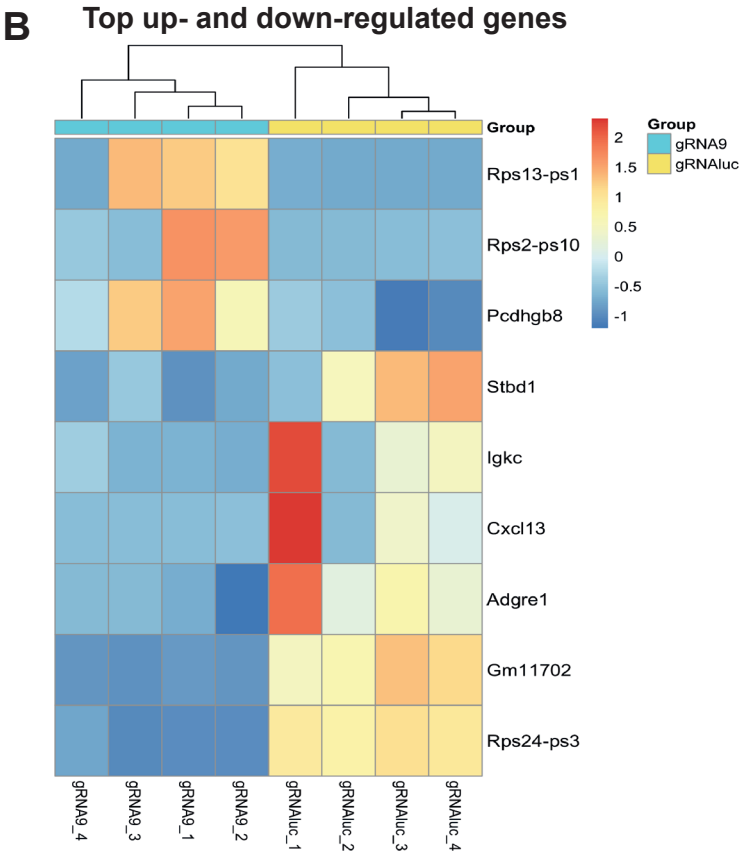
B
Top up- and down-regulated genes
Group
gRNA9
gRNAluc
Rps13-ps1
Rps2-ps10
Pcdhgb8
Stbd1
Igkc
Cxcl13
Adgre1
Gm11702
Rps24-ps3
gRNA9_4
gRNA9_3
gRNA9_1
gRNA9_2
gRNAluc_1
gRNAluc_2
gRNAluc_3
gRNAluc_4

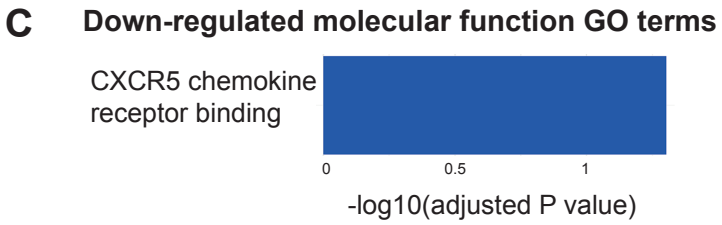
C
Down-regulated molecular function GO terms
CXCR5 chemokine receptor binding
-log10(adjusted P value)

Supplementary Figure 1

A

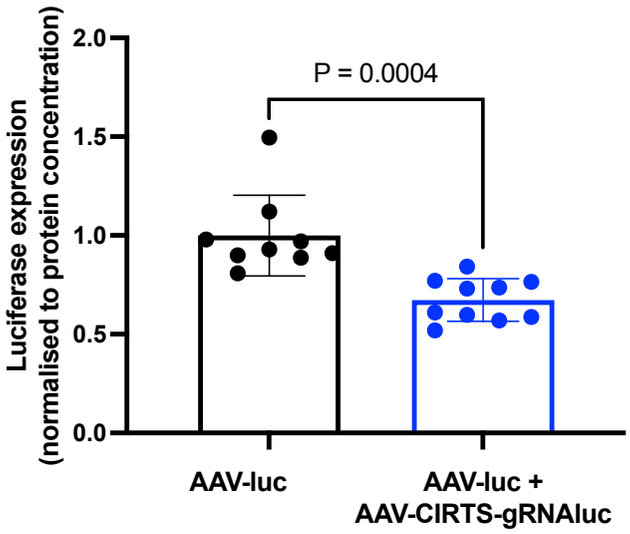

Supplementary Figure 2

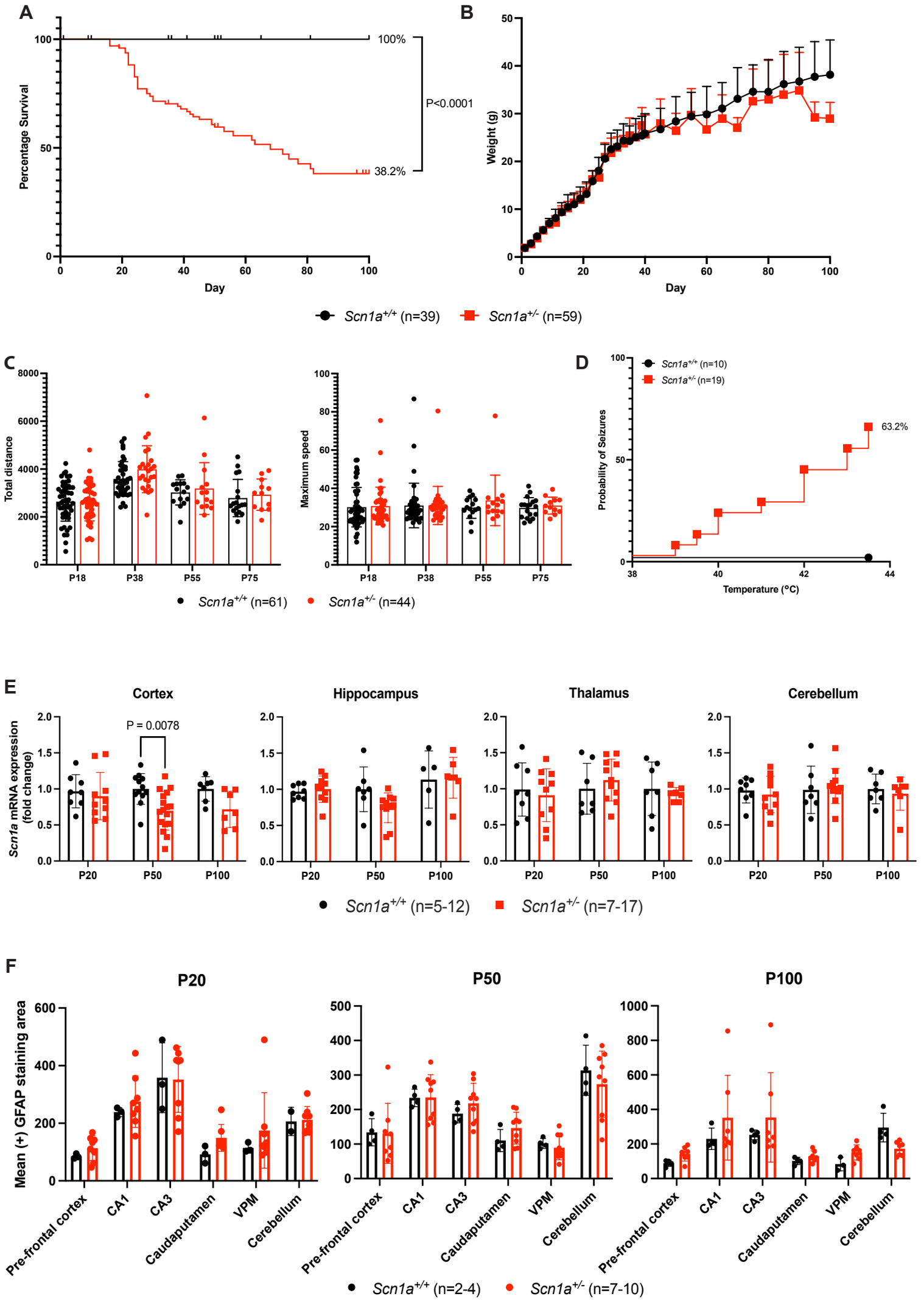

Supplementary Figure 3

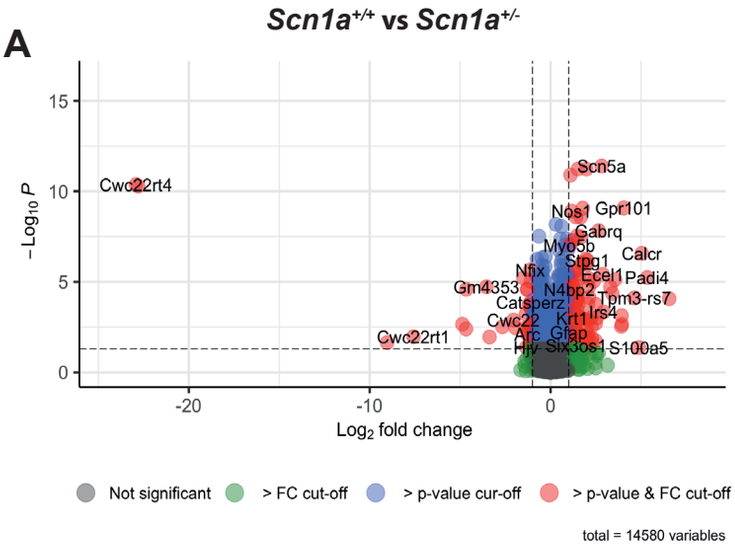

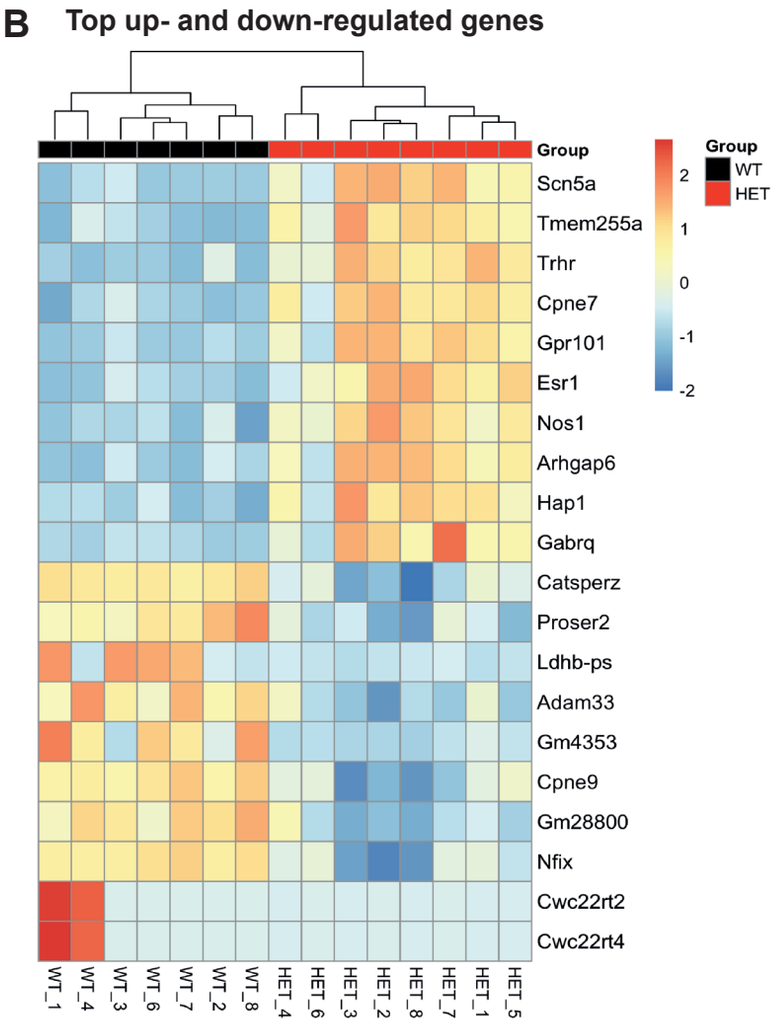

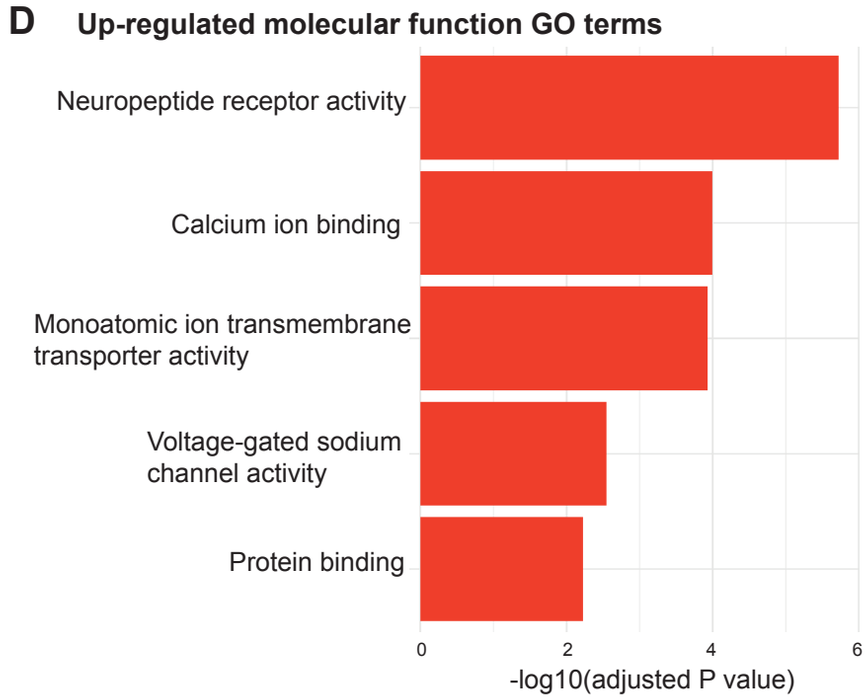

Supplementary Figure 4

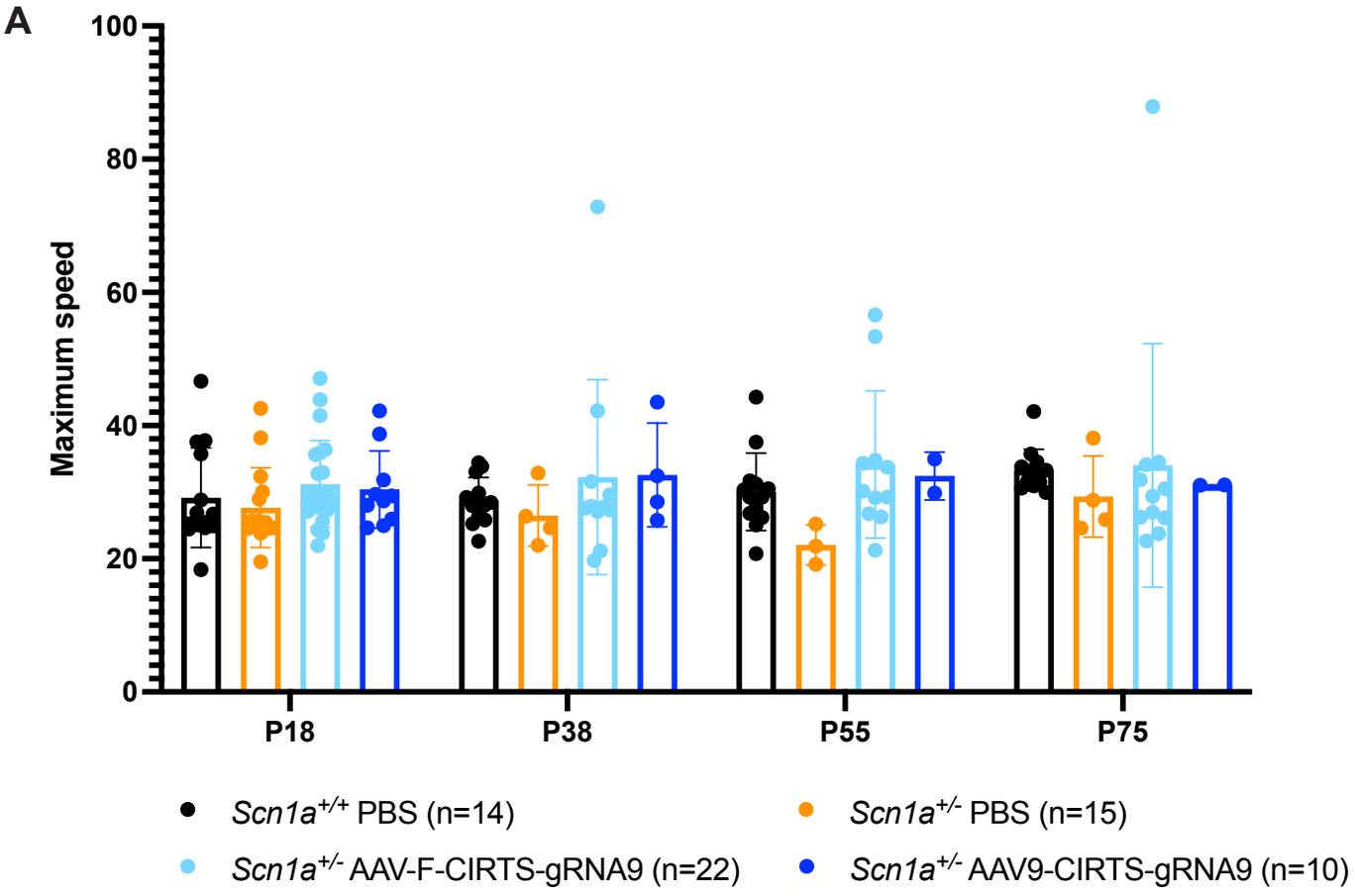

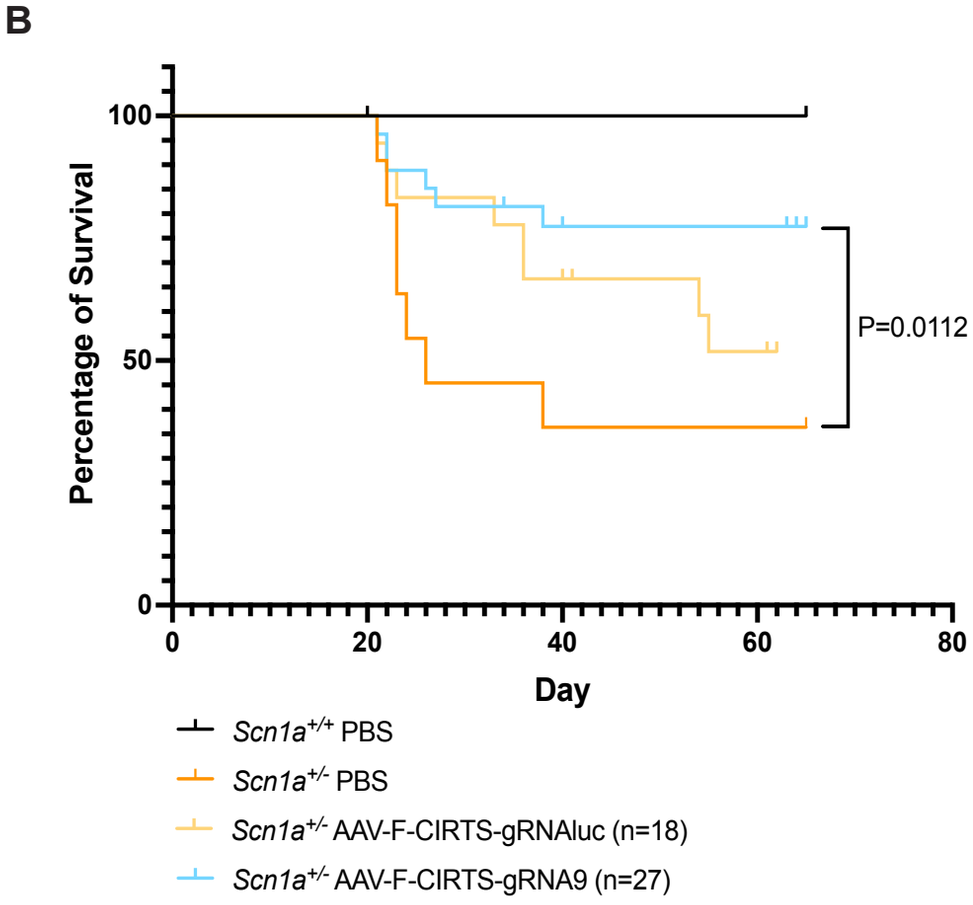

Supplementary Figure 5

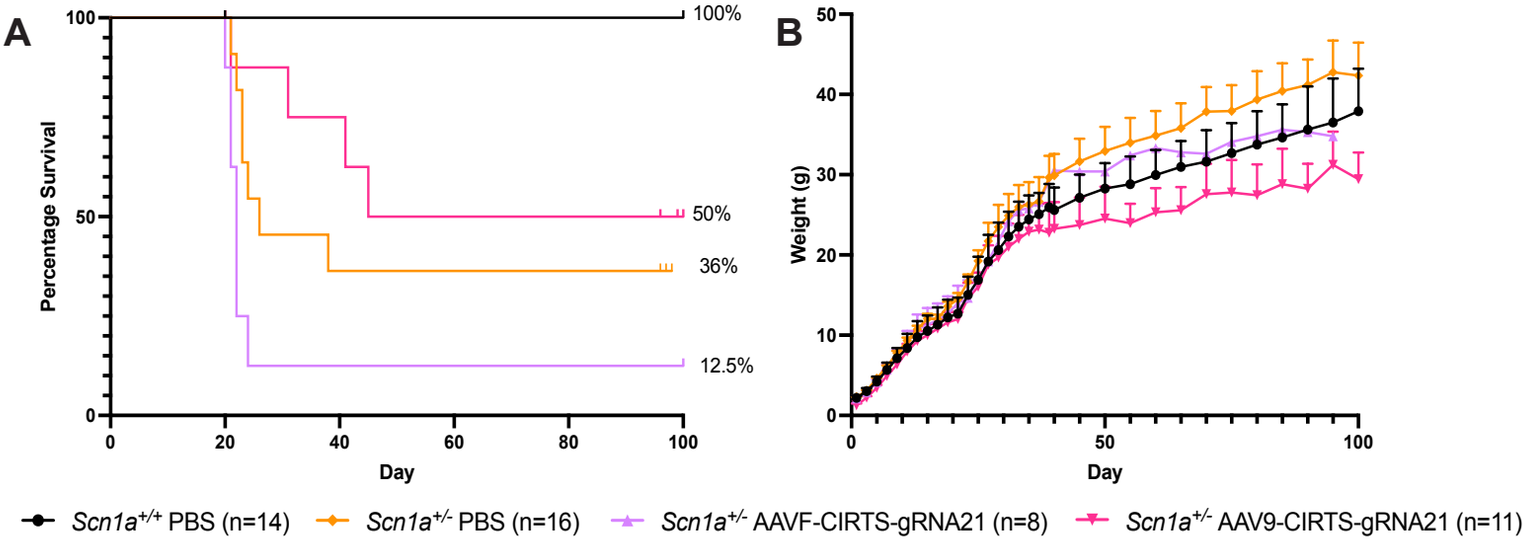

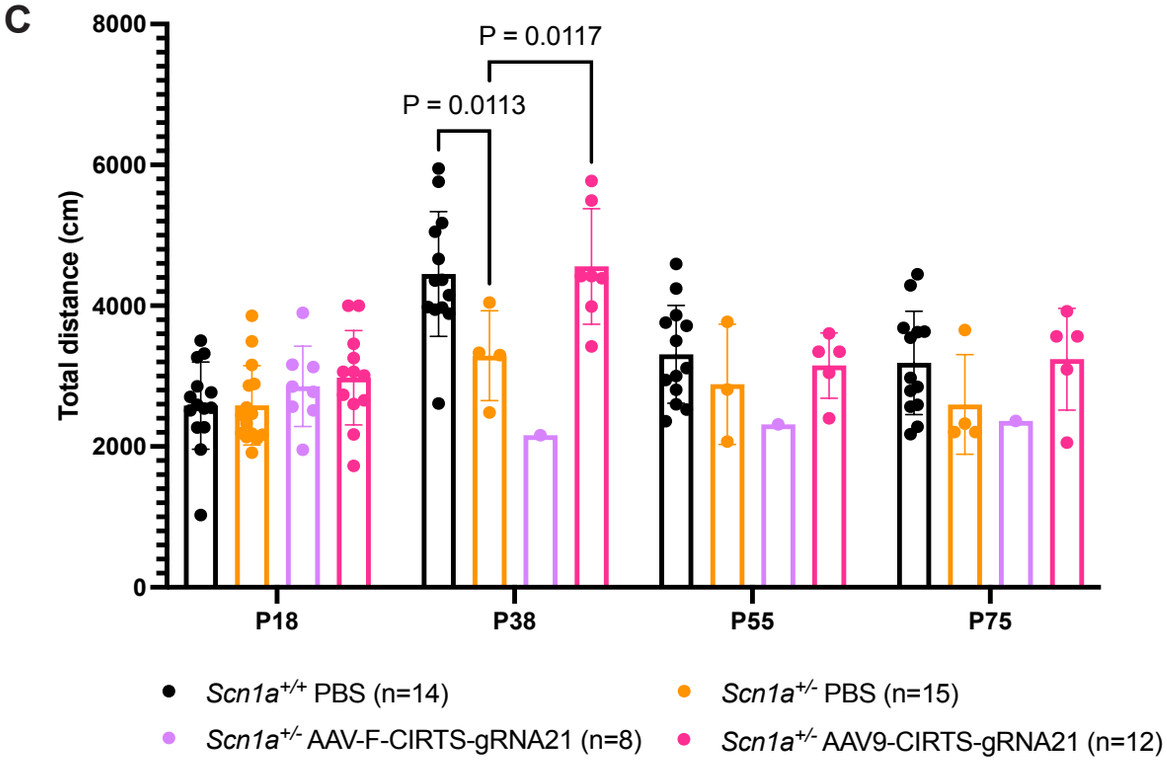

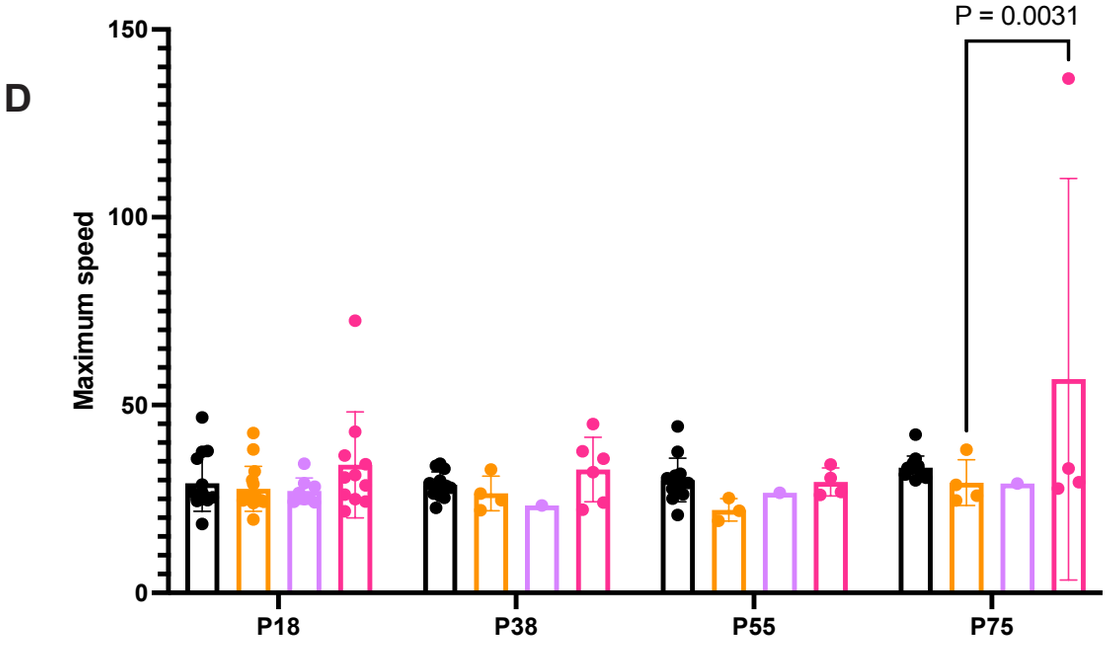

Supplementary Figure 6

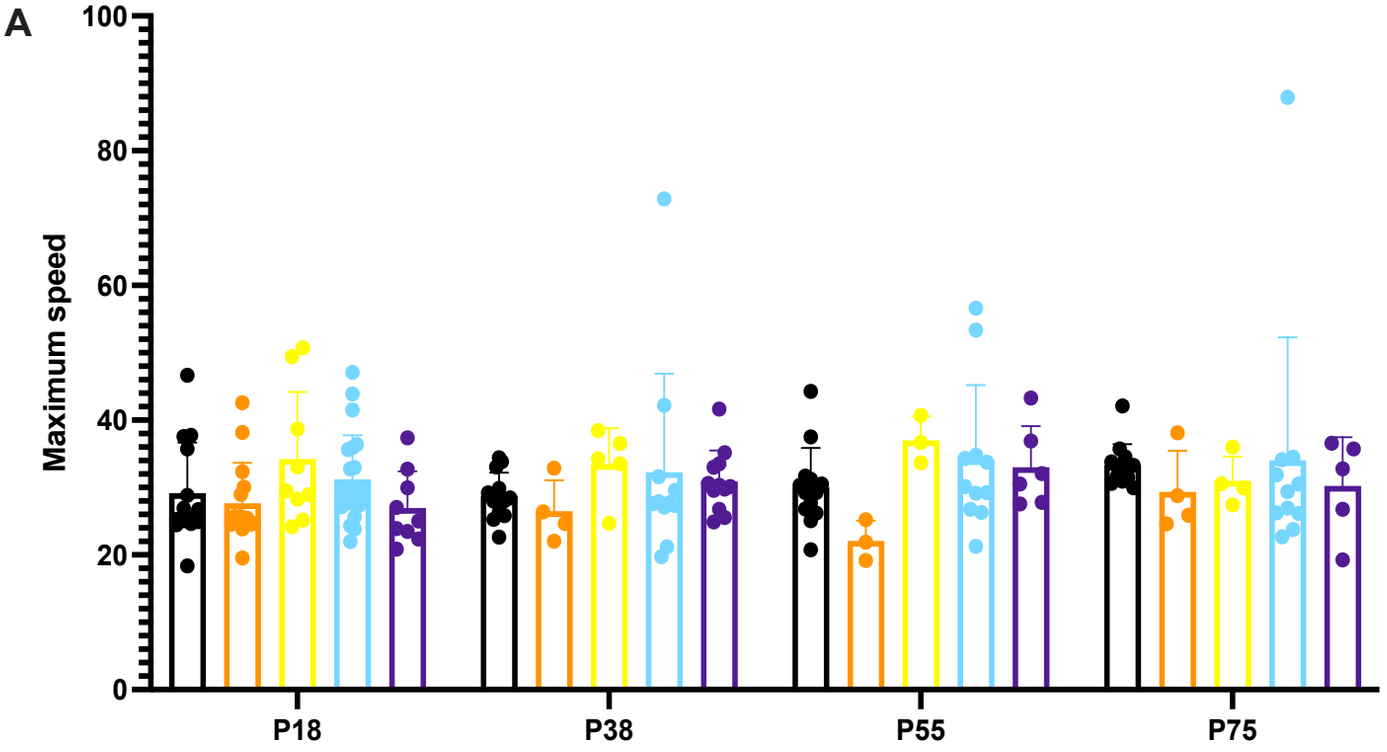

- *Scn1a*$^{+/+}$ PBS (n=14)
- *Scn1a*$^{+/-}$ PBS (n=15)
- *Scn1a*$^{+/-}$ AAV-F-CIRTS-gRNA9 (1.75x10^{10} vg; n=9)
- *Scn1a*$^{+/-}$ AAV-F-CIRTS-gRNA9 (7x10^{10} vg; n=22)
- *Scn1a*$^{+/-}$ AAV-F-CIRTS-gRNA9 (1.75x10^{11} vg; n=12)

Supplementary Figure 7

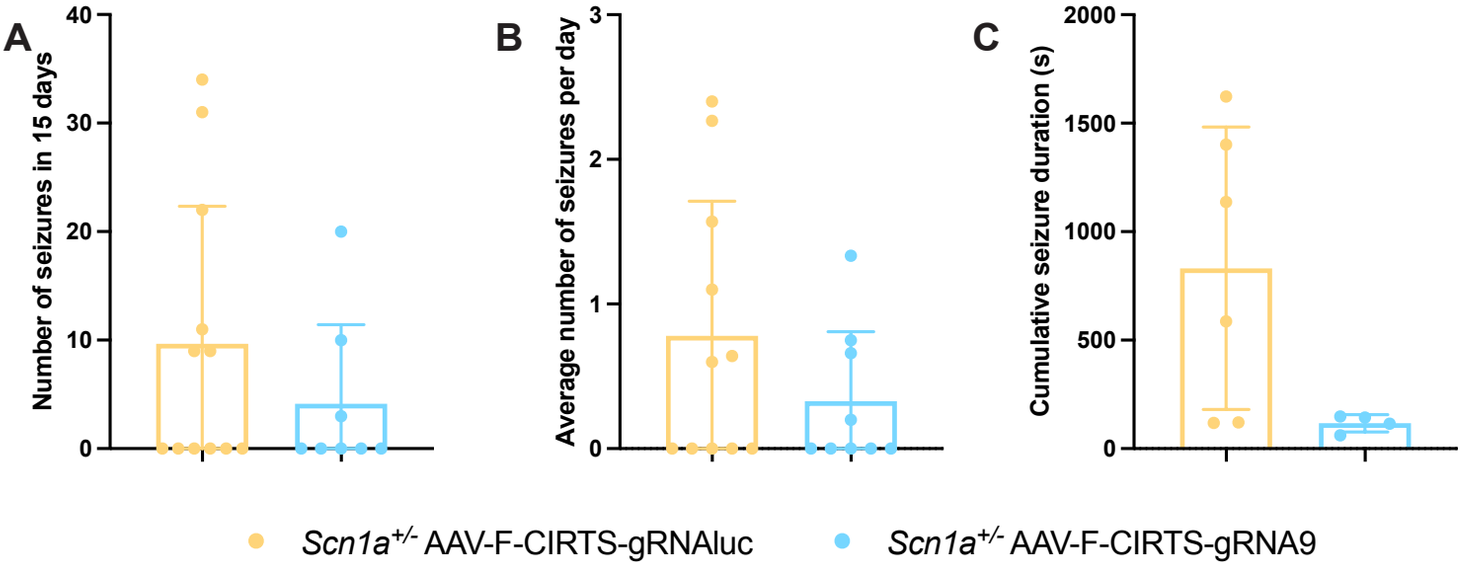

Supplementary Figure 8

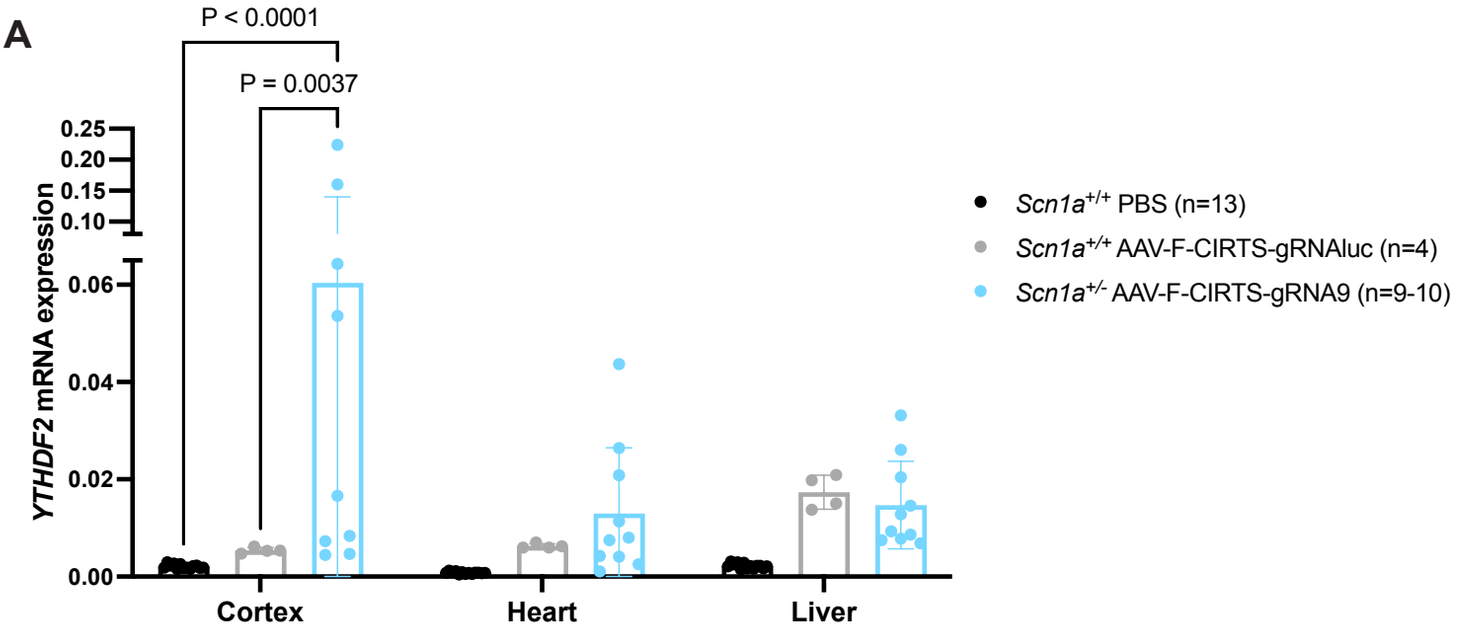
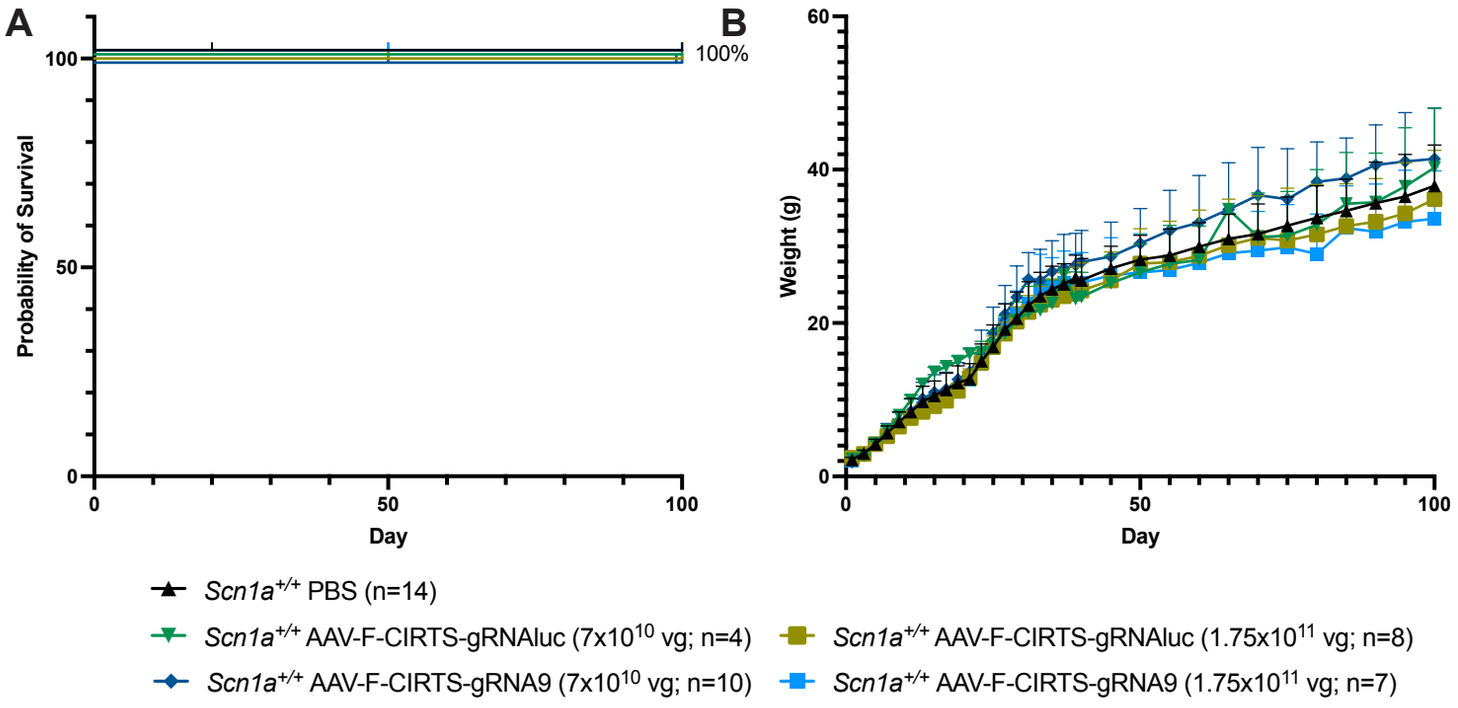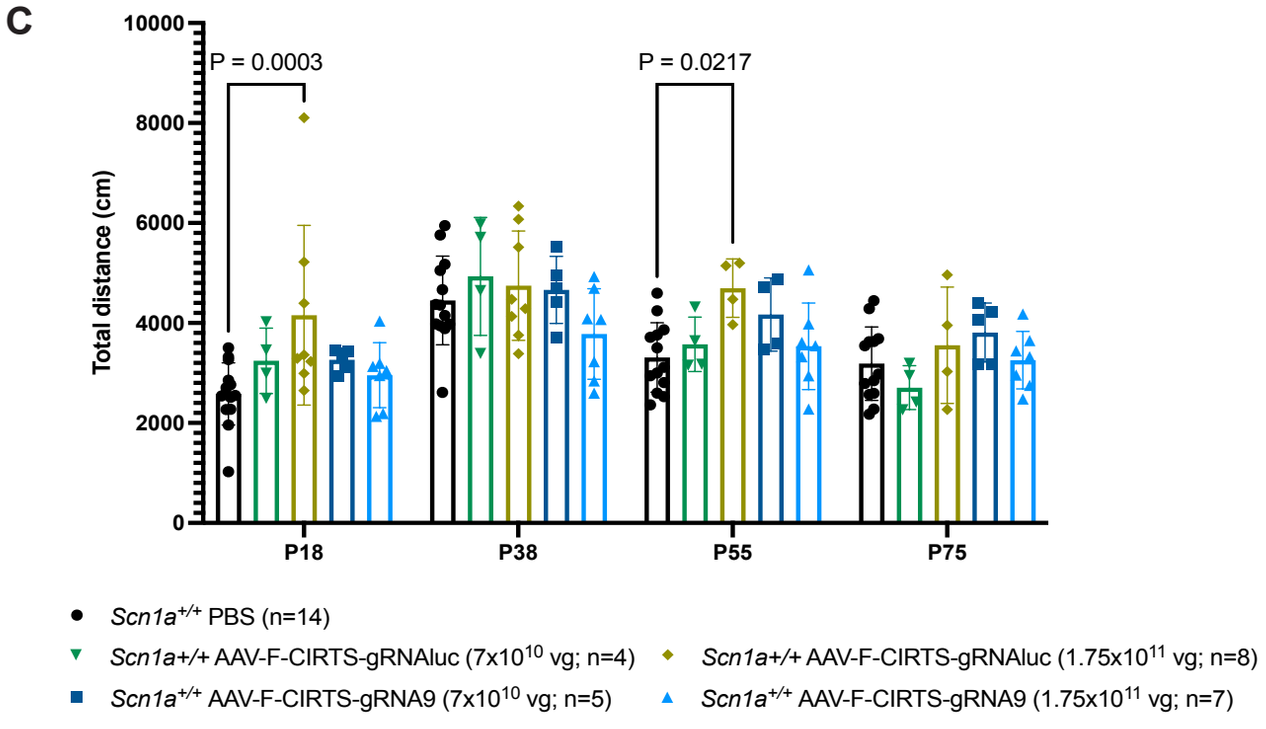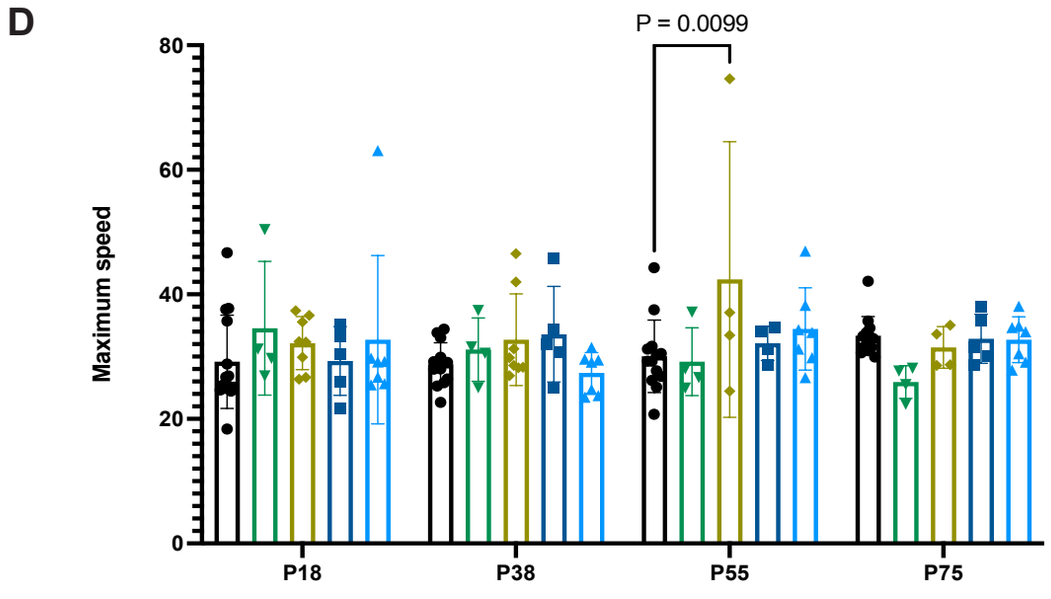
Supplementary Figure 9